JAAS

Journal of Analytical Atomic Spectrometry

Accepted Manuscript

This article can be cited before page numbers have been issued, to do this please use: A. J. McCoy-West, M. Millet, G. Nowell , O. Nebel and K. W. Burton, *J. Anal. At. Spectrom.*, 2020, DOI: 10.1039/C9JA00308H.

View Article Online
DOI: 10.1039/C9JA00308H

ARTICLE

Simultaneous measurement of neodymium stable and radiogenic isotopes from a single aliquot using a double spike

Received 00th January 20xx,
Accepted 00th January 20xx

DOI: 10.1039/x0xx00000x

Alex J. McCoy-West[a,b], Marc-Alban Millet[c], Geoff M. Nowell[b], Oliver Nebel[a], Kevin W. Burton[b]

Neodymium (Nd) stable isotopes have the potential to provide new constraints on a diverse range of geological processes from planetary formation and magmatic differentiation to weathering and ocean circulation. In this contribution, we present a technique for the high-precision measurement of Nd stable isotope ratios by thermal ionisation mass spectrometry (TIMS). We use a ^{145}Nd–^{150}Nd double spike (DS), composed of 28% ^{145}Nd and 67% ^{150}Nd, to correct for mass dependent fractionation resulting from sample preparation and mass spectrometry. Isotope ratios are expressed as δ^{146}Nd which is the per mil deviation in the measured ^{146}Nd/^{144}Nd ratio relative to reference material JNdi-1. Repeated analyses show that an internal precision (n = 400 cycles; 2 se) of ≤0.005‰ on δ^{146}Nd can be achieved in agreement with theoretical predictions. An interlaboratory comparison of the primary standard JNdi-1 over a three-year period shows that resolvable offsets in δ^{146}Nd are induced within and between mass spectrometers as the result of systematic biases in the efficiency of the faraday collectors. Following normalisation of the data to JNdi-1 = 0‰ the long-term reproducibility of δ^{146}Nd on a range of international reference materials processed through chemical separation is better than ±0.015‰ (2 sd). In addition to stable isotope compositions this method allows for the simultaneous measurement of ^{143}Nd/^{144}Nd with a precision of ≤11 ppm. Over a wide range of ^{143}Nd/^{144}Nd (0.5118-0.5132) the DS analyses here agree within analytical uncertainty with published values using conventional techniques. To allow the accurate age correction of these radiogenic isotope compositions in ancient geological samples (>2 Ga) here for the first time we have combined a DS and an elemental tracer spike. A ^{149}Sm tracer spike was calibrated and used to obtain isotope dilution Sm concentrations and ultimately parent-daughter ratios. Measured Sm-Nd ratios are within uncertainty of previous estimates for a range of reference materials, with the addition of the Sm spike having no resolvable effect on δ^{146}Nd values. This technique allows δ^{146}Nd, ^{143}Nd/^{144}Nd and Sm/Nd to be obtained simultaneously, therefore allowing constrains to be placed on both the source or age of a material and the processes involved in its formation.

1. Introduction

Neodymium (Nd; Z = 60) is a refractory (50% condensation temperature = 1594 °C; [1]), lithophile (silicate-loving) element that has been widely utilised to understand the formation and evolution of planet Earth. It has two radiogenic isotopes (^{142}Nd = 27.16%; ^{143}Nd = 12.18%) and five naturally occurring isotopes that can be considered stable on geologically relevant timescales (^{144}Nd, ^{145}Nd, ^{146}Nd, ^{148}Nd and ^{150}Nd with relative abundances of 23.83%, 8.30%, 17.17%, 5.74% and 5.62%, respectively). The long-lived ^{147}Sm-^{143}Nd decay system where ^{147}Sm α decays to ^{143}Nd with a half-life of 106.3 ± 0.5 billion years (Ga) [2, 3] has become an important chronometer and tracer in both high and low temperature geochemistry. Specifically, this radiogenic isotope systems has been utilised to study early solar system dynamics [4-6], planetary differentiation processes [2, 7, 8], mantle heterogeneity [9-12], crustal growth [13-15], mineralization in ore deposits [16], weathering processes [17, 18] and global ocean circulation [19-21]. Samarium (Sm) and Nd are both light rare earth elements (REE) that possess a single valence state (3+) and very similar ionic radii, therefore they exhibit almost identical chemical behaviour. This geochemical similarity coupled with the extremely low REE content of low-temperature fluids (Nd <40 ppt) [22, 23] means that Sm-Nd systematics are generally very robust to secondary modification during metamorphic processes. The other radiogenic isotope ^{142}Nd is the α decay product of the extinct radionuclide ^{146}Sm ($T_{1/2}$ = 103 million years (Ma); [24]) which was only available during the first ca. 500 Ma following Solar System formation. High precision isotope measurements of ^{142}Nd have been used to trace Hadean crustal differentiation events and the preservation of mantle heterogeneities from the earliest period of Earth's history [25-29].

Despite the proliferation of stable isotope geochemistry in the geosciences in recent years, and the potential to use Nd stable isotopes to investigate these same processes, especially under lower temperature conditions, they have received little

[a] School of Earth, Atmosphere and Environment, Monash University, Clayton, Victoria, 3800, Australia.
[b] Department of Earth Sciences, Durham University, Elvet Hill, Durham DH1 3LE, United Kingdom.
[c] School of Earth and Ocean Sciences, Cardiff University, Park Place, Cardiff CF10 3AT, United Kingdom.

† Footnotes relating to the title and/or authors should appear here.
Electronic Supplementary Information (ESI) available: [details of any supplementary information available should be included here]. See DOI: 10.1039/x0xx00000x

attention [30-32]. A potential limitation for the use of Nd stable isotopes in geochemistry is the small range of natural variation expected due to the single valence state of Nd and its high molar mass. Initial efforts by Wakaki and Tanaka[31] used a thermal ionisation mass spectrometry (TIMS) approach to directly analyse a range of synthetic Nd reagents without chemical purification and observed variations of up to 0.3 ‰ in $^{146}Nd/^{144}Nd$. Subsequently, Ma et al.[32] and Saji et al.[33] analysed a small number of terrestrial rock standards using a multi-collector induction coupled plasma mass spectrometry (MC-ICP-MS) standard-sample bracketing technique. Presently, based on a limited sample set variations in $^{146}Nd/^{144}Nd$ up to 0.16 ‰ have been observed in natural materials [30, 32-34].

Obtaining $^{143}Nd/^{144}Nd$, Sm and Nd concentrations from single spiked aliquot following column chemistry is commonly achieved and has been a routine technique in geochemical laboratories for several decades [35]. However, in these cases as $^{146}Nd/^{144}Nd$ is used for mass fractionation correction, stable isotope variations in $^{146}Nd/^{144}Nd$ cannot be quantified. To also obtain $^{143}Nd/^{144}Nd$ isotope ratios Wakaki and Tanaka[31] required two separate TIMS measurements (a spiked and unspiked aliquot) making this methodology labour intensive. To increase the utility of Nd stable isotope analyses here we detail how to obtain stable ($^{146}Nd/^{144}Nd$) and radiogenic ($^{143}Nd/^{144}Nd$) isotope information from a single TIMS measurement and report the current analytical limitations. Within these limits, we propose a protocol that allows constraining the source or age of a material and the processes involved in its formation. Furthermore, to enable application of this technique to several billion-year-old samples, we combined our Nd double spike (a combined isotope tracer enriched in two Nd isotopes, see below) with a Sm tracer spike to obtain high-precision parent-daughter ratios for age correction of $^{143}Nd/^{144}Nd$ isotope ratios. The advantages of processing a single spiked aliquot in terms of limiting sample consumption and providing time and cost savings establish this technique as the ideal method when obtaining stable and radiogenic Nd isotope data.

2. Analytical methods

2.1 Neodymium double spike design

Double spike (DS) is a powerful method that has been shown to be able to efficiently correct for mass dependent isotope fractionation induced during sample digestion, purification and mass spectrometry [36-41], and it has become the technique of choice for the generation of high precision stable isotope ratios when using either MC-ICP-MS or TIMS [30, 31, 39, 42-50]. The composition of the DS implemented here was selected based on the minimum theoretical uncertainty calculated using the double-spike tool box of Rudge et al. (2009) [36]. However, given ^{142}Nd and ^{143}Nd possess radiogenic decay systems these isotopes were not considered when selecting the optimal configuration. Therefore, here we selected a ^{145}Nd-^{150}Nd DS with ^{144}Nd, ^{145}Nd, ^{146}Nd and ^{150}Nd used in the DS inversion, this combination is predicted to have the minimum theoretical uncertainty on DS corrected ratios (ca. 2.5 ppm/amu) and should be accurate over a range of spike–sample mixing proportions (ca. 0.3-0.6; Fig. 1). The DS method was first introduced by Dodson (1963)[37, 38] and in the case of stable isotope ratios consists of resolving a set of three non-linear equations:

$$R_{\mathrm{mes}} = \left[(1-f)R_{\mathrm{std}}\left(\frac{m_x}{m_n}\right)^{\alpha} + fR_{\mathrm{spk}}\right] \mathrm{x} \left(\frac{m_x}{m_n}\right)^{\beta} \quad (1)$$

where R_{mes}, R_{std} and R_{spk} are the measured, standard and spike isotope ratios; m_n is the atomic weight of the normalising isotope (^{144}Nd); m_x is the atomic weight of one of the three other isotopes used to resolve the equation which in our method are ^{145}Nd, ^{146}Nd and ^{150}Nd; f is the relative proportion of ^{144}Nd originating from the spike in the sample–spike mixture; α is the natural fractionation factor between the sample and reference standard, β is the instrumental exponential fractionation factor. In this study Nd stable isotope ratios are expressed as $\delta^{146}Nd$ which is the per mil deviation in the measured $^{146}Nd/^{144}Nd$ relative to the widely measured Geological Survey of Japan Nd reference standard JNdi-1 [51]:

$$\delta^{146/144}\mathrm{Nd} = \left[\left(\frac{\frac{^{146}\mathrm{Nd}}{^{144}\mathrm{Nd}_{\mathrm{Sample}}}}{\frac{^{146}\mathrm{Nd}}{^{144}\mathrm{Nd}_{\mathrm{JNdi-1}}}}\right) - 1\right] \mathrm{x}\ 1000 \quad (2)$$

Although the present magnitude of variations in Nd stable isotopes are relatively small $\delta^{146}Nd$ = 0.3 ‰ [30-33]. We prefer to continue using per mil terminology to avoid confusing these mass dependent variations with the commonly used $\varepsilon^{143}Nd$ and $\mu^{142}Nd$ which are commonly used in the literature when discussing radiogenic Nd isotope variations.

2.2 Calibration of the ^{145}Nd-^{150}Nd double spike

Highly enriched ^{145}Nd (86.7%; enrichment factor (EF) = 10.5) and ^{150}Nd (97.7%; EF = 17.4) spikes were purchased as fine-grained metallic powders from Trace Sciences International, Canada. The spikes were digested individually using concentrated triple distilled HNO_3. The individual spikes were subsequently mixed in the calculated optimal proportions and resulting double spike was diluted in 3M HNO_3 to the desired concentration (2.576 ppm). Calibration of the Nd DS was achieved by measuring pure standard and DS solutions as well as a range of JNdi-1–DS mixtures. Practically, this involves iterative correction for instrumental mass fractionation of the pure DS measurements to generate a putative true DS composition, with an initial estimate provided by the pure JNdi-1 analysis. This putative true DS composition is then fed into the DS deconvolution and used on all JNdi-1–DS mixtures, ranging from 0.1:0.9 to 0.9:0.1 mixing proportions. The calibration is considered satisfactory once most mixtures, especially those around the optimum mixture proportions, display a $\delta^{146}Nd$ within an estimated analytical uncertainty of zero. Measurements were carried out using Triton Plus TIMS at Durham University with each analysis comprising 500 cycles of 8.39 seconds. The isotope composition of the DS and of reference standard JNdi-1, as used in the calibration and stable isotope calculations, can be found in Table 1.

2.3 Calibration of a ^{149}Sm tracer spike

An enriched ^{149}Sm (95.1%; EF = 6.88) tracer was purchased as fine-grained metallic powder from Isoflex, USA. The spike was digested using concentrated triple distilled HNO_3 and subsequently diluted in 3M HNO_3 to the desired concentration (0.483 ppm). The isotopic composition of the spike was determined using the external normalisation method following the calculations of Wasserburg et al. (1981)[35]. Around 400 ng of the reference material High Purity Standards 1000 ppm Sm solution was measured using static

Journal of Analytical Atomic Spectrometry ARTICLE

View Article Online
DOI: 10.1039/C9JA00308H

collection mode without normalisation. The Sm standard shows a consistent percentage of fractionation per atomic mass unit (amu) of ca. 0.03 %, with respect to the recommended values [52]. Using these fractionation factors the measured composition of the Sm spike can then be externally normalised. Here we employ the exponential fractionation law as it is considered to more satisfactorily account for the instrumental fractionation than a linear or power law [35]. Measurements were carried out by Triton Plus TIMS at Monash University with each analysis comprising 300 cycles of 8.39 seconds. The isotope composition of the ^{149}Sm tracer spike and of reference standard used in the calibration and isotope dilution calculations, can be found in Table 2. These results represent the average of two separate filaments for both the standard and spike solution.

2.4 Sample preparation and chemical purification of Nd (and Sm)

2.4.1 Sample selection and digestion

In this study we present analyses of three pure Nd standard solutions, JNdi-1, La Jolla and a new in-house Monash University Nd standard (Mona) which is a solution of High Purity Standards 1000 ppm Nd solution (Lot# 1601901). Along with repeated analyses of three United States Geological Survey rock standards (BHVO-2, BIR-1 and G-2) and two National Institute of Standards and Technology glasses (SRM NIST-612 and SRM NIST-614). This data is supplemented with measurements of five intraplate basalts from the Lookout Volcanics, Marlborough, New Zealand [11].

In preparation for the chemical separation of Nd and Sm up to 0.2g of the reference materials (rock powder or glass) was careful weighed into pre-cleaned 15 mL Savillex Teflon beakers. This amount varied from ca. 20-40 mg (BHVO-2, G-2, NIST-612), ca. 70-90 mg (BIR-1), ca. 100-170 mg (NIST-614) depending on the Nd concentration of sample. The Lookout Volcanics samples used in this study were coarse crushates (0.5-1.0 mm) of the original whole rocks and to ensure homogeneity a large quantity (ca. 300-400 mg) was dissolved. For samples with ≤200 ng of natural Nd the ^{145}Nd-^{150}Nd DS was added based on ideal sample to spike ratio of 60:40 (Fig. 1) along with the ^{149}Sm tracer spike (using an ideal $^{149}Sm_{spike}$-$^{149}Sm_{sample}$ of 2.5). The samples were then dissolved using a concentrated HF-HNO_3 (3:1) mixture on a hotplate at ≥130 °C for 72 hours. To ensure complete dissolution the samples were sequentially brought into solution in concentrated HNO_3 (x2) and HCl and refluxed on a hotplate for at least 24 hours. For samples with significantly more than 200 ng of Nd (BHVO-2, G-2, NIST-612) following complete dissolution the samples were bought into solution 5 mL 6M HCl, and aliquots containing ca. 200 ng were then weighed into a separate 15 mL Savillex beakers and spiked using the ^{145}Nd-^{150}Nd DS and ^{149}Sm spike for isotope dilution. To ensure complete spike-sample equilibration these solutions were then refluxed on a hotplate at 120 ºC in 2 mL concentrated HNO_3 for at least 4 hours and dried down overnight. Dissolved and equilibrated samples are brought into solution in 2 mL of 1M HCl and refluxed overnight at 100 °C ready for separation of Nd from the rock matrix.

2.4.2 Chromatographic Separations

Neodymium was separated following a combination of well-established chromatographic techniques [10, 30, 53]. In this study the rare earth elements (REE) were separated from the sample matrix using Bio-Rad Polyprep columns (2.0 mL resin capacity) filled with Bio-Rad AG50W-x8 (100-200 mesh) cation exchange resin as described in McCoy-West et al. (2017) [30]. Prior to chemistry the columns were cleaned with at least 2-3 columns loads of 6M HCl (ca. 20 mL). The samples were transferred into precleaned 2 mL polypropylene centrifuge vials and then centrifuged for 5 min at 10,000 rpm. For cleaning vials were submerged in 1M HNO_3 for at least 1 month, and then rinsed 3 times with MQ H_2O and dried. Centrifuged samples (2 mL of 1M HCl) are then carefully loaded onto the top of the resin bed. The matrix was then sequentially removed in 10 mL 1M HCl + 1M HF, 12 mL 2.5M HCl and 8 mL 2M HNO_3 with the REE fraction collected in 13 mL of 6M HCl. The yield of Nd from these columns is ≥97.5 % (n = 3; calculated based on the proportion of Nd counts in the collected 6M HCl fraction, relative to the total number of Nd counts in all fractions obtained from the column, including cleaning following collection, as measured by ICP-MS).

The REE fraction was then dried and Nd and Sm were separated from the other REE using polypropylene columns (length = 88 mm; internal diameter = 4 mm) filled with Eichrom Ln-Spec resin (50-100 µm) based on the methods of Pin and Zalduegui (1997)[53]. Prior to chemistry the columns were cleaned with 3 columns loads of 6M HCl (ca. 12 mL). Samples were loaded in 0.5 mL of 0.2M HCl, another 6 mL of 0.2M HCl was then eluted, prior to the collection of Nd in the next 6 mL of 0.2M HCl. To collect Sm a further 2 mL of 0.4M HCl was then eluted, prior to the collection of Sm in 2.5 mL of 0.4M HCl. Neodymium and Sm cuts were then evaporated to dryness overnight at 95 ºC in preparation for mass spectrometry. This separation protocol results in perfect separation of Sm (isobaric interferences on ^{144}Nd, ^{148}Nd, and ^{150}Nd) from Nd (see Fig. 2), with the yield of Nd from these columns ≥99%. Residual Ce can be present in the Nd cut (ca. 2%; isobaric interference on ^{142}Nd), and therefore ^{142}Nd /^{144}Nd ratios are not reported here. Furthermore, the calibration of the DS is not precise enough to enable the natural variations in terrestrial ^{142}Nd/^{144}Nd to be resolved. Total procedural blanks over a 2-year period measured by isotope dilution vary from 1-15 pg (Avg. = 6; n = 9) at Durham and 33-55 pg (n = 2) at Monash and in all cases were negligible. To confirm that this chromatographic procedure had no effect on the stable Nd isotopic ratios repeat aliquots of the JNdi-1 standard were passed through the complete chemical procedure and the δ^{146}Nd value obtained is indistinguishable within uncertainty from that of unprocessed aliquots [30].

2.5 Mass spectrometry and data processing

2.5.1 Neodymium isotope measurements by TIMS

Neodymium isotope measurements were performed using Thermo-Fisher Triton Plus TIMS at the Arthur Holmes Geochemistry Labs, Durham University and Isotopia Laboratory, Monash University. In preparation for loading and TIMS analysis the solutions were evaporated to dryness at 120 ºC in 3 drops of 16M HNO_3, samples were then individually loaded using 1 µL of 16M HNO_3 onto Re ionisation filaments using a double filament assembly. The total Nd content of the synthetic solutions analysed in this study varies from 100-200 ng. Whereas, with the unknowns standard practice is to load the complete sample that general consist of 200 ng of natural Nd (i.e. without the spike component). Neodymium was measured as a metal ion in static collection mode using eight faraday collectors using the main cup configuration shown in Table 3 (^{146}Nd in the axial cup). Samarium was monitored at ^{147}Sm and used to correct for isobaric interferences on ^{144}Nd, ^{148}Nd and ^{150}Nd. Ideal analyses comprised 20 blocks of 20 scans with an integration time of 8.4 seconds (400 cycles = 60 min). Due to the large Nd loads

View Article Online DOI: 10.1039/C9JA00308H

samples can be warmed-up reasonably quickly ca. 15-20 min, taking the total analysis time per sample to just under 1 hour 30 min.

2.5.2 Neodymium isotope deconvolution

The DS deconvolution procedure applied in this study was undertaken using the Wolfram Mathematica program and follows the algebraic resolution method described by Millet and Dauphas (2014)[45]. To obtain the final δ-values requires simultaneously resolving a set of three non-linear equations (see Eq. 1). Uncertainty on the calculated δ-values have been propagated using a Monte Carlo simulation in order to account for the correlated uncertainties on the ion beam intensities of the different isotopes analysed. Practically, 2000 data points are simulated based on the covariance matrix of all ion beams considered in the double spike deconvolution. A δ-value is then calculated for each of them, and the final uncertainty on δ^{146}Nd is taken as the 2 standard error of all values. These calculations have been confirmed using the Isospike deconvolution program of Creech and Paul (2015)[54], which is based on the algebraic equations presented in Rudge et al. (2009)[36], and the geometric iterative resolution method of Siebert et al. (2001)[39], all three approaches yield identical results within analytical uncertainty (with a maximum offset ≤4 ppm) [30].

As Nd has greater than four isotopes and because the radiogenic isotope ^{143}Nd is not used during DS deconvolution, the spike proportion, and the geological and analytical fractionation factors resolved during deconvolution can be used to calculate the ^{143}Nd/^{144}Nd ratio of the samples from the same analysis. This methodology has previously been employed [30, 43] but here we describe the equations used:

$$\frac{^{143}\mathrm{Nd}}{^{144}\mathrm{Nd}_{\mathrm{mes}}} = \left[(1-f)\ \mathrm{x}\ \left(\frac{^{143}\mathrm{Nd}}{^{144}\mathrm{Nd}_{\mathrm{JNdi-1}}}\mathrm{x}\left(\frac{m_{143}}{m_{144}}\right)^{\alpha} + Rad143\right) + \left(f\ \mathrm{x}\frac{^{143}\mathrm{Nd}}{^{144}\mathrm{Nd}_{\mathrm{spk}}}\right)\right] \times \left(\frac{m_{143}}{m_{144}}\right)^{\beta} \quad (3)$$

With the parameters being defined in same manner as in Eq. 1. Eq.3 introduces a new variable, *Rad143*, which represents the departure of the ^{143}Nd/^{144}Nd ratio from mass dependent fractionation relationship with JNdi-1. In other words, it represents the difference in the amount of radiogenic ^{143}Nd between sample and JNdi-1. Importantly, *Rad143* can display either positive or negative values. This equation can be solved simultaneously with the other three equations of the DS system.

Finally, because all radiogenic isotope data is reported to a given stable isotope composition (i.e. ^{146}Nd/^{144}Nd = 0.7219 [55]) The final fractionation corrected ^{143}Nd/^{144}Nd of the sample can then be calculated:

$$\frac{^{143}\mathrm{Nd}}{^{144}\mathrm{Nd}_{\mathrm{dfc}}} = \frac{^{143}\mathrm{Nd}}{^{144}\mathrm{Nd}_{\mathrm{JNdi-1}}} + Rad143\ \mathrm{x}\left(\frac{m_{143}}{m_{144}}\right)^{-\alpha} \quad (4)$$

Furthermore, to provide an additional check of quality of the analyses the δ^{148}Nd, which is the per mil deviation relative to the widely measured reference standard JNdi-1 has also been calculated:

$$\delta^{148/144}\mathrm{Nd} = \left[\left(\frac{^{148}\mathrm{Nd}}{^{144}\mathrm{Nd}_{\mathrm{mes}}}\right)\Big/\left(\frac{m_{148}}{m_{144}}\right)^{\beta} - \frac{f\ \mathrm{x}\ \frac{^{148}\mathrm{Nd}}{^{144}\mathrm{Nd}_{\mathrm{Spk}}}}{\frac{1-f}{\frac{^{148}\mathrm{Nd}}{^{144}\mathrm{Nd}_{\mathrm{JNdi-1}}}}} - 1\right] \mathrm{x}\ 1000 \quad (5)$$

In this instance the isotopic ratios are not assumed to follow a mass dependent relationship as opposed to ^{145}Nd/^{144}Nd, ^{146}Nd/^{144}Nd and ^{150}Nd/^{144}Nd during the primary DS deconvolution which opens the possibility to investigate kinetic effects in low temperature systems if the fractionations are large enough.

Therefore, using the equations above it is possible to obtain δ^{146}Nd, δ^{148}Nd, ^{143}Nd/^{144}Nd and the Nd concentration of a sample from a single TIMS measurement.

2.5.3 Samarium measurements by MC-ICP-MS

Samarium isotope dilution measurements were performed using Thermo-Fisher Neptune Plus MC-ICP-MS in the Isotopia Laboratory at Monash University. Samples were introduced using an Aridus II desolvating nebuliser and Cetac100 nebuliser (aspiration rate ca. 100 µlmin^{-1}). All measurements were made in low resolution using H-cones, and static collection mode using the cup configuration shown in Table 3. Isobaric interferences on Sm from Nd and Gd were monitored at ^{146}Nd (interferes on ^{144}Sm, ^{148}Sm and ^{150}Sm) and ^{155}Gd (interferes on ^{152}Sm and ^{154}Sm) and used to correct for these isobaric interferences. These corrections were always negligible with generally <10^{-5} V of the interfering elements. Standard operation involved introduction of 10 ppb Sm solutions in 2% HNO_3 to undertake tuning and produced a maximum sensitivity was ~540 Vppm^{-1}. Each analysis consisted of 1 block of 50 cycles with an integration time of 2.1 s, with a washout of at least 120 s occurring after each sample. Isotope dilution calculations to remove the composition of the spike were undertaken iteratively (at least 5 cycles) offline in Microsoft Excel. Any potential isobaric interference from ^{150}Nd added by the Nd DS are avoided because the Sm spike subtraction calculations do not consider this mass (instead using ^{147}Sm, ^{148}Sm, ^{149}Sm and ^{152}Sm).

3. Results and discussion

This study reports ^{143}Nd/^{144}Nd and δ^{146}Nd, δ^{148}Nd and Nd and Sm concentrations and Sm-Nd ratios with results presented in Tables 4 and 5 (see also supplement). All internal uncertainties are quoted as 2 standard error (2 se), whereas long-term reproducibility is given using 2 standard deviations (2 sd) to show population variability, with the uncertainty on long-term averages given as 95% standard errors (95% se =*t* x sd/(n)$^{1/2}$, where *t* = inverse survival function of the Student's t-test at the 95% significance level and (n −1) degrees of freedom).

3.1 Interlaboratory comparison and long-term reproducibility of δ^{146}Nd

3.1.1 Variations in the composition of JNdi-1 over time and between mass spectrometers

This study presents data collected over a two-year period at Durham University and then subsequently almost 1 year at Monash University using the same DS and solution of JNdi-1 (Fig. 3; Supplementary Table 1). On every analysis day following the calibration of the amplifier gains a JNdi-1 analysis was undertaken. At Durham University from Nov 2016 to Nov 2017 the δ^{146}Nd of

Journal of Analytical Atomic Spectrometry ARTICLE

JNdi-1 hovers around 0 ‰ with an average composition of 0.004 ± 0.002 ‰ (n = 64). From January 2018 onwards, a new higher average value is then observed of δ^{146}Nd = 0.019 ± 0.003 ‰ (n = 36). In December 2017 an ion pump on the flight tube of Triton Plus at Durham University was replaced, resulting in the instrument being completed vented and then baked out, which can lead to degradation of the faraday collectors. At Monash University analyses of JNdi-1 from Sept 2018 to July 2019 show a distinctly different composition that is resolvably lighter than zero with δ^{146}Nd = −0.023 ± 0.003 ‰ (n = 15).

To investigate the cause of the systematic offsets in JNdi-1 two further tests where undertaken: 1) rotating the amplifiers; and 2) changing the cup configuration.

To assess whether the inaccuracy in δ^{146}Nd was the result of an uncorrected bias from differences in the amplifier gains, analyses using amplifier rotation were conducted. These analyses used 300 ng of JNdi-DS mixture and consisted of 16 blocks of 40 cycles with 30 seconds of background measured between each block, resulting in two complete cycles of amplifier rotation. These 640 cycles analyses had a total analysis time of 1 hour 50 mins. The average δ^{146}Nd of these analyses was −0.024 ± 0.004 ‰ (n = 3) and is identical within uncertainty to the other analyses at Monash (Fig. 3; Supplementary Table 1). Therefore, it can be concluded that the offset in JNdi-1 is unrelated to the amplifier assignment.

To assess whether the inaccuracy in δ^{146}Nd is the result of an uncorrected bias between the faraday collectors' analyses using a different collector configuration were conducted. These analyses use the secondary cup configuration (with ^{145}Nd in the axial cup) where all the measured masses have been shifted one collector heavier as presented in Table 3. Analyses of JNdi-1 at Monash using this secondary cup configuration and 400 cycles of static collection produce a resolvable heavier δ^{146}Nd of −0.012 ± 0.003 ‰ (n = 6; Fig. 3). This difference confirms that the small offset between labs is the result of systematic uncorrected bias in the collection efficiency of the faraday collectors themselves. To obtain ultra-precise sub ±5 ppm data (2 sd), analysts in the ^{142}Nd community routinely apply a range of dynamic cup-configuration routines to correct for variations in faraday cup efficiency [56, 57]. This approach requires at least two magnet steps are made that move both the target and a standardizing isotope into the same faraday cup [56], these dynamic collection routines typically rely on a 1 amu shift between lines. Given that the analyses herein use a DS that contains ^{150}Nd to correct for systematic bias between the faraday collectors using dynamic multi-collector analyses would require getting ^{150}Nd and ^{144}Nd into the same collector while simultaneously measuring the other isotope is considered impractical (basically impossible) due to mass dispersion (6 amu) of these isotopes. Even if a dynamic routine could be developed the extensive amount of extra analysis time to generate this level of precision (±5 ppm; 2 sd) is not considered necessary for Nd stable isotopes analyses when total variations in δ^{146}Nd so far measured are around 330 ppm in synthetic materials and 160 ppm in natural samples (herein; [30, 31, 33]).

3.1.2 Secondary normalisation of δ^{146}Nd values

Figure 3 clearly shows that differences exist between different TIMS instruments, but also, they can be generated within a single mass spectrometer due to uncorrected inefficiencies between the faraday collectors. The relative deterioration of faraday collectors and their change in efficiency through time has been recognised as a source of inaccuracy in the determination of isotope ratios by static multi-collection since the 1990s [55, 58]. If these offsets were the result of the degradation of the faraday collectors a linear drift in the δ^{146}Nd of JNdi-1 with time would be expected. In this case both Triton Plus TIMS are relatively new and especially at Monash (installed in June 2017 with limited usage) significant decay of the faraday collectors is not considered possible. Instead in this instance these offsets are clearly resolvable (± 20 ppm) relative to the precision of the analyses, but also appear systematic and stable over an extend period while the instrument configuration is left undisturbed.

During our initially work the long-term average of δ^{146}Nd in JNdi-1 was within uncertainty of zero, and therefore a correction was not considered necessary [30]. By definition the primary reference standard used to calculate δ-values should have a composition of 0 ‰ (in this instance JNdi-1). Therefore, to correct for the offsets in δ^{146}Nd values between analytical configurations, δ^{146}Nd values of unknowns have been corrected to a composition of JNd-1 = 0‰ based on the long-term offset of the JNdi-1 in the period in question. Uncertainties were propagated in quadrature using the measured 2 se of the analysis and 95% se on the long-term average of the JNdi-1 from a specific period. Applying a correction such as this is common practice for radiogenic ^{143}Nd/^{144}Nd isotope data (e.g. [10, 11, 27, 59]). Furthermore, it is common place to correct DS stable isotope data generated by MC-ICP-MS [45, 50, 60-62]in this manner to deal with small amounts of non-exponential mass bias that is not accounted for by internal corrections methods. The normalisation applied here is no different.

Prior to applying this normalisation, measurements at the two universities produce resolvably different δ^{146}Nd values (Fig. 4b), with the long-term reproducibility (2 sd) of the USGS rock standards varying from ±0.023 to ±0.039 ‰ in δ^{146}Nd. . However, once this normalisation is applied, the long-term reproducibility improves significantly to be ≤ ±0.015 ‰ (15 ppm; see below for further discussion) with measurements at Durham and Monash generally falling with analytical uncertainty of each other (Fig. 4a). Moving forward, other labs planning to undertake these analyses should endeavour to build a strong record of standard analyses to assess any systematic bias in their data relative to the composition of the primary reference standard used.

3.1.3 Internal precision, external reproducibility and accuracy of δ^{146}Nd

Internal precision of δ^{146}Nd on a single analysis is generally between 0.004 to 0.007 ‰ (2 se; Fig. 5), although some larger uncertainties occur due to mass spectrometer instability or when analysing smaller amounts of Nd (e.g. for chondrites [30]). The amount of Nd on the analysed filament (and therefore the signal intensity generated) clearly influences the uncertainty of an analysis with 100 ng aliquots of JNdi-1 producing a significantly higher proportion of uncertainties that are greater than 0.008%, than larger 200 ng aliquots (Fig. 5b).

Repeated measurements of the synthetic standard solutions La Jolla (δ^{146}Nd = −0.214 ±0.010‰; n = 7; Table 4) and Mona (δ^{146}Nd = +0.116 ±0.012‰; n = 8) at Monash University over a 9-month period gave a reproducibility of ≤ ±0.012‰ (Fig. 6). The stable Nd isotope analyses of La Jolla herein are within uncertainty of that previously reported (δ^{146}Nd = −0.197 ±0.023‰; n = 2 [31]).

The long-term reproducibility of the technique was tested further through repeated digestions of a range of reference materials. Multiple digestions of BHVO-2, BIR-1 and G-2 were

undertaken at both Durham and Monash Universities. Following normalisation to JNdi-1 = 0‰ for the systematic offset generated by relative collector inefficiency (see discussion above; Fig. 3) all the rock standards reproduce better than ±0.015‰ (Fig. 4; Table 5). This is comparable to that achieved previously based on repeated measurements of BHVO-1 at Durham University (Fig. 4; [30]). Analyses of multiple digestions of the synthetic glasses NIST-612 also produced highly consistent results with δ^{146}Nd = −0.150 ±0.013‰ (Fig. 6). No resolvable difference is observed between the Nd stable isotope composition of aliquots processed with and without the Sm-tracer spike (Figs. 5 & 6). Due to the excellent chemical separation of Nd and Sm with this protocol (Fig. 2), we can be confident that addition of the Sm-spike has no measurable effect on δ^{146}Nd values. Taken together, these data suggest that the long-term reproducibility of the δ^{146}Nd measurements is ≤ ±0.015‰.

There is currently a very limited database of δ^{146}Nd values on reference materials [30, 32, 33]. However, analyses obtained without the use of a double spike are prone to inaccuracy due to incomplete Nd yields during chemical separation (e.g. [32]; see [30] for further discussion). Wakaki and Tanaka (2012)[31] showed significant mass dependent variations can be artificially induced during column chromatography (seven fractions of JNdi-1 had δ^{146}Nd that varied from 0.46‰ at the beginning to −0.94‰ at the end of Nd collection) consequently it is imperative to obtain 100% yield when not using a double spike. A secondary check on the accuracy of the δ^{146}Nd values obtained from the analyses here is provided by the ^{143}Nd/^{144}Nd and δ^{148}Nd which are discussed further below.

3.2 Obtaining accurate and precise radiogenic isotope and parent-daughter ratios

3.2.1 Accuracy and external reproducibility of ^{143}Nd/^{144}Nd

The ^{143}Nd/^{144}Nd values obtained following DS deconvolution here can be compared directly to previously published values for the same samples (Fig. 7). Over a wide range of ^{143}Nd/^{144}Nd from 0.5118 to 0.5132 and for a diverse selection of materials (basalts, rock standards, synthetic glass, synthetic solutions) the analyses here generally agree with published values [11, 55, 63, 64] within analytical uncertainty (Fig. 7a). For example the rock standards BHVO-2, BIR-1 and G-2 have been measured with ^{143}Nd/^{144}Nd of 0.512982 ±10, 0.513088 ±11 and 0.512226 ±7, respectively, which are all within uncertainty of published values (Table 5; [11, 53, 63, 65-67]). The long-term reproducibility of DS ^{143}Nd/^{144}Nd measurements is comparable to conventional TIMS analyses [10, 55] with reference standards (rocks and glass) measured at least 10 times have uncertainties of ≤ ±0.000011. An initial discrepancy was observed relative to the values reported for NIST-612 in GeoReM[68] (^{143}Nd/^{144}Nd = 0.51193). But, when the primary references [69, 70] were checked and those data were normalised (by up to 20 ppm) to identical standard values as used herein the previously published data (^{143}Nd/^{144}Nd = 0.511911 ±13) agrees within uncertainty to values obtained herein (see Fig. 7c; Table 5). This reinforces the point that normalisation to a constant reference values is imperative when undertaking interlaboratory comparisons. The excellent accuracy of the ^{143}Nd/^{144}Nd obtained following DS deconvolution also provides strong evidence that the δ^{146}Nd values obtained here are accurate.

3.2.2 Accuracy and precision of Sm-Nd ratios

Obtaining accurate Sm-Nd ratios is imperative when using the isochron method to undertake Sm-Nd dating, or when applying an age correction to ^{143}Nd/^{144}Nd data in very old (>2 Ga) samples. The Sm/Nd obtained here using a mixed Sm tracer and Nd DS are in excellent agreement with previously published values [11, 53, 63, 71, 72] (Fig. 7b; Supplementary Table 4). The analysed samples (basalts, rock standards, synthetic glass) possess a wide range of Sm/Nd from 0.20 to 1.06 but are all within uncertainty of previously published values (Table 5). For example, both BHVO-2 (Sm/Nd = 0.250 ±0.002; n =7) and NIST-612 (Sm/Nd = 1.062 ±0.003; n =7) agree with uncertainty to previous estimates (0.248 ±0.004 and 1.062 ±0.003, respectively; [63, 71]). The excellent agreement with previous values on well characterised materials (i.e. NISTSRM glass [71]) and long-term reproducibility of Sm/Nd (≤ ±0.004; 0.3%) obtained here will enable accurate and precise age corrections to be applied to ^{143}Nd/^{144}Nd data, even for extremely old samples, in the future using this methodology.

3.3 Confirming mass dependence using δ^{148}Nd

If at least three isotopes of an analyte exist when using conventional standard-sample bracketing MC-ICP-MS analyses it is possible to calculate a secondary isotope ratio (i.e., ^{67}Zn/^{64}Zn combined with ^{66}Zn/^{64}Zn [73]) to confirm the instrumental mass dependent fractionation of the analysis in question. Normally when adding a DS this is no longer possible because the DS corrects for mass fractionation during mass spectrometry and in the process the calculated isotope compositions are assumed to follow a mass dependence fractionation on a kinetic fractionation law. Recent work has shown that obtaining a second stable isotope ratio provides the possibility to assess whether isotope fractionations are the results of equilibrium or kinetic processes (e.g., Mg and Fe; [73-75]). For Nd given it has seven stable isotopes, after excluding the four isotopes used in the DS deconvolution (^{144}Nd, ^{145}Nd, ^{146}Nd and ^{150}Nd) and the two radiogenic nuclides (^{142}Nd and ^{143}Nd), ^{148}Nd remains the only available isotope. As shown in Eq. (4) it is possible to calculate the $\delta^{148/144}$Nd of an analysis following the DS deconvolution. For a wide range of materials $\delta^{148/144}$Nd values are generally ca. twice the δ^{146}Nd values (Fig. 8), with the majority of analyses falling near the mass dependent fractionation line (Slope = 2.00037) and within the long-term reproducibility of $\delta^{148/144}$Nd (±0.038‰). The long-term uncertainty on $\delta^{148/144}$Nd is calculated from the reproducibility of δ^{146}Nd (±0.015‰) but has been increased proportionally based on the relative mass difference between the isotopes and the less precise counting statistics due to the smaller ion beam of ^{148}Nd. The only samples that fall outside this uncertainty envelope are rare analyses of chondritic meteorites which given their origins may contain components with significant isotopic heterogeneities due to nucleosynthetic effects (Fig. 8). The high atomic mass (z = 60) of Nd results in a relative mass difference that is relatively small (for ^{144}Nd/^{146}Nd: Δm/m = 1.38 %), so it is expected that to distinguish any kinetic isotope effects large variations in δ^{146}Nd will be required. Based on observations with other stable isotope systems where large non-equilibrium isotope fractionation occur the best places to search for these effects will be in low-temperature terrestrial systems (e.g. biological effects) or the individual components of meteorites (e.g. CAIs). The presented method should, in theory, be applicable to these environments and may be used to reveal such effects in future studies.

3.4 Nd stable isotopes in geological materials

The absolute abundances of the REE, including Nd, have been extensively used to study magmatic processes, including fractional crystallisation, partial melting and crustal assimilation [11, 76, 77].

Journal of Analytical Atomic Spectrometry ARTICLE

Given that stable isotope fractionation is process dependent variations in isotopic ratios can also be used to provide new insights into these fundamental processes. Although the samples analysed presently for Nd stable isotopes do not represent a co-magmatic suite, their varied whole rock compositions allow first order inferences to be made on the effects of magmatic differentiation on δ^{146}Nd (Fig. 9). Samples with basaltic to dacitic major element compositions (SiO_2 = 38-69 wt %; herein and [30]) generally show limited variability in δ^{146}Nd with an average composition of δ^{146}Nd = −0.028 ± 0.011‰ (2 sd; n = 15). Interestingly, sample BIR-1 (δ^{146}Nd = 0.013 ± 0.015‰) does not conform to this simple story, but this sample has also been shown to possess a unique light Ti isotope composition [45]. At higher SiO_2 contents the two most felsic rocks analysed display heavier δ^{146}Nd at SiO_2 above 70 wt % (RGM-1: SiO_2 = 73 wt %; δ^{146}Nd = −0.010 ± 0.007‰ and JG-2: SiO_2 = 76 wt %; δ^{146}Nd = 0.010 ± 0.004‰; Supplementary Table 3). Presumably the enrichment of heavy Nd in these high-SiO_2 samples results from the crystallisation or removal of accessory, REE-bearing mineral phases. Monazite, allanite xenotime, titanite and apatite can all incorporate significant amounts of light REE relative to whole-rock concentrations (≥100-1000 fold; [78, 79]), therefore a change in coordination environment between these minerals and the coexisting melt would be capable of generating stable isotope fractionations. At equilibrium stable isotope theory would predict that at a fixed valance state, heavy isotopes will preferentially enter the site with the stiffest bonds (i.e. lowest coordination number; [80]). Experimental work suggests that Nd (and the LREE) are predominantly 7-fold coordinated in silicate and other oxide glasses [81, 82], whereas in monazite, the predominant REE host in granitic magmas, Nd resides within a distorted octahedra (NdO_9; [83]) with a coordination number of 9. Thus, during magmatic differentiation light isotopes would preferentially enter the accessory phase, with removal of these crystals driving the residual melt to heavier δ^{146}Nd (as observed in Fig. 9). Clearly, magmatic processes are capable of modifying Nd stable isotopic compositions although at present the full extent and magnitude of these fractionations remain unconstrained.

The Lookout Volcanics represent the oldest sampling (98 Ma [84]) of the HIMU(high $^{238}U/^{204}Pb$)-like ($^{206}Pb/^{204}Pb$ >20.5 [11]) magmatic mega-province of the southwest Pacific. The sub-continental lithospheric mantle in this region underwent widespread carbonatite metasomatism [11, 76, 85], which is still an ongoing process [10]. Despite this intense metasomatism the Lookout Volcanics have an unremarkable composition (Fig. 9) with an average composition of δ^{146}Nd = −0.022 ± 0.007‰ (2 sd; n = 5), which is indistinguishable from most analysed magmatic rocks with <50 wt % SiO_2. If heterogeneities do exist in lithospheric mantle due to carbonatite metasomatism, they may not be observed here due the failure to sample those metasomes during melting or homogenisation of this signature as melting proceeds. Investigations of Nd stable isotopes are just beginning, and only with additional work will we uncover what this isotope system has to offer.

4. Conclusions

Here we present a method for the high-precision measurement of Nd stable isotopes by TIMS which enables determination of δ^{146}Nd, $^{143}Nd/^{144}Nd$ and the Sm-Nd ratio of a sample from a single spiked aliquot. This method utilises a ^{145}Nd–^{150}Nd DS, with the effects of adding a ^{149}Sm tracer spike also investigated. As a result of uncorrectable biases between individual faraday collectors resolvable offsets in δ^{146}Nd between different analytical setups can be distinguished. Following normalisation to JNdi-1 = 0‰ the long-term reproducibility of δ^{146}Nd on a range of international reference materials processed through chemical separation is better than ±0.015‰. This precision is based on large Nd loads (ca. 200 ng) and will deteriorate when smaller samples are processed. We recommend other labs seeking to undertake similar analyses continuously analyse the primary reference material JNdi-1 to enable data normalisation to be undertaken accurately.

In addition to stable isotope compositions this method allows the concurrent measurement of $^{143}Nd/^{144}Nd$. Over a wide range of $^{143}Nd/^{144}Nd$ the DS analyses obtained here agree within analytical uncertainty of published values using conventional techniques. The addition of ^{149}Sm tracer spike has also enabled Sm-Nd ratios to be obtained, which agree with published estimates for a range of reference materials. This demonstrates that this technique will allow accurate and precise age correction of $^{143}Nd/^{144}Nd$ in ancient geological samples. Despite direct isobaric interferences the addition of the Sm spike has no resolvable effect on δ^{146}Nd values due to the excellent chemical separation of Nd and Sm. The coupled analysis of stable δ^{146}Nd and radiogenic $^{143}Nd/^{144}Nd$ as presented here will allow: 1) the processes involved in the formation of a reservoir; and 2) the composition of its precursor materials to be assessed simultaneously. Neodymium stable isotope geochemistry remains in its infancy and only with further work will the full potential of this technique be realised.

Conflicts of interest

The authors declare no conflicts of interest.

Acknowledgements

AMW thanks all the people who have provided mentoring in geochemical techniques over the last decade as this knowledge coalesced to aid the completion of this work. Yona Nebel-Jacobsen is thanked for maintenance of the facilities at Monash University. Ashlea Wainwright is thanked for discussions on dynamic TIMS routines. This research was supported by NERC Grant (NE/M0003/1) to KWB and ARC grant FL160100168 to Peter Cawood. Insightful reviewers from 3 anonymous referees help improve the clarity of the manuscript.

References

1. K. Lodders, *The Astrophysical Journal*, 2003, **591**, 1220-1247.
2. G. W. Lugmair and K. Marti, *Earth and Planetary Science Letters*, 1978, **39**, 349-357.
3. O. A. P. Tavares and M. L. Terranova, *Applied Radiation and Isotopes*, 2018, **139**, 26-33.
4. R. Andreasen and M. Sharma, *Science*, 2006, **314**, 806.
5. A. Bouvier and M. Boyet, *Nature*, 2016, **537**, 399-402.
6. C. Burkhardt, L. E. Borg, G. A. Brennecka, Q. R. Shollenberger, N. Dauphas and T. Kleine, *Nature*, 2016, **537**, 394-398.

7. S. B. Jacobsen and G. J. Wasserburg, *Earth and Planetary Science Letters*, 1984, **67**, 137-150.
8. R. W. Carlson and G. W. Lugmair, *Earth and Planetary Science Letters*, 1988, **90**, 119-130.
9. E. Jagoutz, R. W. Carlson and G. W. Lugmair, *Nature*, 1980, **286**, 708-710.
10. A. J. McCoy-West, V. C. Bennett and Y. Amelin, *Geochimica et Cosmochimica Acta*, 2016, **187**, 79-101.
11. A. J. McCoy-West, J. A. Baker, K. Faure and R. Wysoczanski, *Journal of Petrology*, 2010, **51**, 2003-2045.
12. A. Stracke, A. W. Hofmann and S. R. Hart, *Geochemistry Geophysics Geosystems*, 2005, **6**.
13. D. J. DePaolo, *Geochimica et Cosmochimica Acta*, 1980, **44**, 1185-1196.
14. M. T. McCulloch and V. C. Bennett, *Geochimica et Cosmochimica Acta*, 1994, **58**, 4717-4738.
15. S. B. Jacobsen, *Geochimica et Cosmochimica Acta*, 1988, **52**, 1341-1350.
16. J. T. Chesley, A. N. Halliday and R. C. Scrivener, *Science*, 1991, **252**, 949-951.
17. B. Öhlander, J. Ingri, M. Land and H. Schöberg, *Geochimica et Cosmochimica Acta*, 2000, **64**, 813-820.
18. D. Vance and K. Burton, *Earth and Planetary Science Letters*, 1999, **173**, 365-379.
19. F. Albarède and S. L. Goldstein, *Geology*, 1992, **20**, 761-763.
20. C. Jeandel, T. Arsouze, F. Lacan, P. Téchiné and J. C. Dutay, *Chemical Geology*, 2007, **239**, 156-164.
21. T. van de Flierdt, S. L. Goldstein, S. R. Hemming, M. Roy, M. Frank and A. N. Halliday, *Earth and Planetary Science Letters*, 2007, **259**, 432-441.
22. M. Bau, *Chemical Geology*, 1991, **93**, 219-230.
23. A. Michard and F. Albarède, *Chemical Geology*, 1986, **55**, 51-60.
24. F. Meissner, W. D. Schmidt-Ott and L. Ziegeler, *Zeitschrift für Physik A Atomic Nuclei*, 1987, **327**, 171-174.
25. G. Caro, B. Bourdon, J.-L. Birck and S. Moorbath, *Nature*, 2003, **423**, 428.
26. M. Boyet and R. W. Carlson, *Science*, 2005, **309**, 576-581.
27. V. C. Bennett, A. D. Brandon and A. P. Nutman, *Science*, 2007, **318**, 1907.
28. H. Rizo, M. Boyet, J. Blichert-Toft, J. O'Neil, M. T. Rosing and J.-L. Paquette, *Nature*, 2012, **491**, 96.
29. N. S. Saji, K. Larsen, D. Wielandt, M. Schiller, M. M. Costa, M. J. Whitehouse, M. T. Rosing and M. Bizzarro, *Geochemical Perspectives Letters*, 2018, **7**, 43-48.
30. A. J. McCoy-West, M.-A. Millet and K. W. Burton, *Earth and Planetary Science Letters*, 2017, **480**, 121-132.
31. S. Wakaki and T. Tanaka, *International Journal of Mass Spectrometry*, 2012, **323–324**, 45-54.
32. J. Ma, G. Wei, Y. Liu, Z. Ren, Y. Xu and Y. Yang, *Journal of Analytical Atomic Spectrometry*, 2013, **28**, 1926-1931.
33. N. S. Saji, D. Wielandt, C. Paton and M. Bizzarro, *Journal of Analytical Atomic Spectrometry*, 2016, **31**, 1490-1504.
34. A. J. McCoy-West and K. W. Burton, *AGU Fall Meeting Abstracts*, 2017, 2017AGUFM.P2053F..2006M.
35. G. J. Wasserburg, S. B. Jacobsen, D. J. DePaolo, M. T. McCulloch and T. Wen, *Geochimica et Cosmochimica Acta*, 1981, **45**, 2311-2323.
36. J. F. Rudge, B. C. Reynolds and B. Bourdon, *Chemical Geology*, 2009, **265**, 420-431.
37. M. H. Dodson, *Geochimica et Cosmochimica Acta*, 1970, **34**, 1241-1244.
38. M. H. Dodson, *Journal of Scientific Instruments*, 1963, **40**, 289-295.
39. C. Siebert, T. F. Nägler and J. D. Kramers, *Geochemistry, Geophysics, Geosystems*, 2001, **2**, 1032.
40. S. G. John, *Journal of Analytical Atomic Spectrometry*, 2012, **27**, 2123-2131.
41. B. Hamelin, G. Manhes, F. Albarede and C. J. Allègre, *Geochimica et Cosmochimica Acta*, 1985, **49**, 173-182.
42. E. C. Inglis, J. B. Creech, Z. Deng and F. Moynier, *Chemical Geology*, 2018, **493**, 544-552.
43. J. A. M. Nanne, M.-A. Millet, K. W. Burton, C. W. Dale, G. M. Nowell and H. M. Williams, *Journal of Analytical Atomic Spectrometry*, 2017, **32**, 749-765.
44. M.-A. Millet, N. Dauphas, N. D. Greber, K. W. Burton, C. W. Dale, B. Debret, C. G. Macpherson, G. M. Nowell and H. M. Williams, *Earth and Planetary Science Letters*, 2016, **449**, 197-205.
45. M.-A. Millet and N. Dauphas, *Journal of Analytical Atomic Spectrometry*, 2014, **29**, 1444-1458.
46. B. L. A. Charlier, G. M. Nowell, I. J. Parkinson, S. P. Kelley, D. G. Pearson and K. W. Burton, *Earth and Planetary Science Letters*, 2012, **329**, 31-40.
47. P. Bonnand, I. J. Parkinson, R. H. James, A.-M. Karjalainen and M. A. Fehr, *Journal of Analytical Atomic Spectrometry*, 2011, **26**, 528-535.
48. J. Creech, J. Baker, M. Handler, M. Schiller and M. Bizzarro, *Journal of Analytical Atomic Spectrometry*, 2013, **28**, 853-865.
49. L. Gall, H. Williams, C. Siebert and A. Halliday, *Journal of Analytical Atomic Spectrometry*, 2012, **27**, 137-145.
50. A. J. McCoy-West, P. Chowdhury, K. W. Burton, P. Sossi, G. M. Nowell, J. G. Fitton, A. C. Kerr, P. A. Cawood and H. M. Williams, *Nature Geoscience*, 2019, DOI: 10.1038/s41561-019-0451-2.
51. T. Tanaka, S. Togashi, H. Kamioka, H. Amakawa, H. Kagami, T. Hamamoto, M. Yuhara, Y. Orihashi, S. Yoneda, H. Shimizu, T. Kunimaru, K. Takahashi, T. Yanagi, T. Nakano, H. Fujimaki, R. Shinjo, Y. Asahara, M. Tanimizu and C. Dragusanu, *Chemical Geology*, 2000, **168**, 279-281.
52. M. Berglund and E. Wieser Michael, *Journal*, 2011, **83**, 397.
53. C. Pin and J. S. Zalduegui, *Analytica Chimica Acta*, 1997, **339**, 79-89.
54. J. B. Creech and B. Paul, *Geostandards and Geoanalytical Research*, 2015, **39**, 7-15.
55. M. F. Thirlwall, *Chemical Geology*, 1991, **94**, 85-104.
56. M. Garçon, M. Boyet, R. W. Carlson, M. F. Horan, D. Auclair and T. D. Mock, *Chemical Geology*, 2018, **476**, 493-514.
57. M. F. Horan, R. W. Carlson, R. J. Walker, M. Jackson, M. Garçon and M. Norman, *Earth and Planetary Science Letters*, 2018, **484**, 184-191.
58. A. Makishima and E. Nakamura, *Chemical Geology*, 1991, **94**, 105-110.
59. A. J. McCoy-West, V. C. Bennett, I. S. Puchtel and R. J. Walker, *Geology*, 2013, **41**, 231-234.
60. Y. Li, A. J. McCoy-West, S. Zhang, D. Selby, K. W. Burton and K. Horan, *Economic Geology*, 2019, **114**, 981-992.
61. R. A. Neely, S. R. Gislason, M. Ólafsson, A. J. McCoy-West, C. R. Pearce and K. W. Burton, *Earth and Planetary Science Letters*, 2018, **486**, 108-118.
62. M.-A. Millet, J. A. Baker and C. E. Payne, *Chemical Geology*, 2012, **304–305**, 18-25.

Journal of Analytical Atomic Spectrometry ARTICLE

View Article Online
DOI: 10.1039/C9JA00308H

63. K. P. Jochum, U. Weis, B. Schwager, B. Stoll, S. A. Wilson, G. H. Haug, M. O. Andreae and J. Enzweiler, *Geostandards and Geoanalytical Research*, 2016, **40**, 333-350.
64. H. Rizo, M. Boyet, J. Blichert-Toft and M. Rosing, *Earth and Planetary Science Letters*, 2011, **312**, 267-279.
65. D. Weis, B. Kieffer, C. Maerschalk, J. Barling, J. de Jong, G. A. Williams, D. Hanano, W. Pretorius, N. Mattielli, J. S. Scoates, A. Goolaerts, R. M. Friedman and J. B. Mahoney, *Geochemistry, Geophysics, Geosystems*, 2006, **7**, Q08006.
66. C.-F. Li, Z.-Y. Chu, J.-H. Guo, Y.-L. Li, Y.-H. Yang and X.-H. Li, *Analytical Methods*, 2015, **7**, 4793-4802.
67. C. Pin and A. Gannoun, *Analytical Chemistry*, 2017, **89**, 2411-2417.
68. K. P. Jochum, U. Nohl, K. Herwig, E. Lammel, B. Stoll and A. W. Hofmann, *Geostandards and Geoanalytical Research*, 2005, **29**, 333-338.
69. M. Ganio, K. Latruwe, D. Brems, P. Muchez, F. Vanhaecke and P. Degryse, *Journal of Analytical Atomic Spectrometry*, 2012, **27**, 1335-1341.
70. J. D. Woodhead and J. M. Hergt, *Geostandards Newsletter*, 2001, **25**, 261-266.
71. K. P. Jochum, U. Weis, B. Stoll, D. Kuzmin, Q. Yang, I. Raczek, D. E. Jacob, A. Stracke, K. Birbaum, D. A. Frick, D. Günther and J. Enzweiler, *Geostandards and Geoanalytical Research*, 2011, **35**, 397-429.
72. C.-F. Li, X.-H. Li, Q.-L. Li, J.-H. Guo, X.-H. Li, L.-J. Feng and Z.-Y. Chu, *Analytical Chemistry*, 2012, **84**, 6040-6047.
73. A. J. McCoy-West, J. Godfrey Fitton, M.-L. Pons, E. C. Inglis and H. M. Williams, *Geochimica et Cosmochimica Acta*, 2018, **238**, 542-562.
74. E. D. Young and A. Galy, *Reviews in Mineralogy and Geochemistry*, 2004, **55**, 197-230.
75. M. Olsen, B. , M. Schiller, A. N. Krot and M. Bizzarro, *The Astrophysical Journal Letters*, 2013, **776**, L1.
76. A. J. McCoy-West, V. C. Bennett, H. S. C. O'Neill, J. Hermann and I. S. Puchtel, *Journal of Petrology*, 2015, **56**, 563-604.
77. C. J. Allègre and J. F. Minster, *Earth and Planetary Science Letters*, 1978, **38**, 1-25.
78. R. A. Exley, *Earth and Planetary Science Letters*, 1980, **48**, 97-110.
79. W. N. Sawka, *Earth and Environmental Science Transactions of the Royal Society of Edinburgh*, 1988, **79**, 157-168.
80. E. A. Schauble, *Reviews in Mineralogy and Geochemistry*, 2004, **55**, 65-111.
81. K. J. Rao, J. Wong and M. J. Weber, *The Journal of Chemical Physics*, 1983, **78**, 6228-6237.
82. M. M. Mann and L. G. DeShazer, *Journal of Applied Physics*, 1970, **41**, 2951-2957.
83. Y. Ni, J. M. Hughes and A. N. Mariano, *American Mineralogist*, 1995, **80**, 21-26.
84. A. J. McCoy-West, M.Sc., MSc thesis, Victoria University of Wellington, 2009.
85. C. Timm, K. Hoernle, R. Werner, F. Hauff, P. v. den Bogaard, J. White, N. Mortimer and D. Garbe-Schönberg, *Earth Science Reviews*, 2010, **98**, 38-64.
86. A. S. G. Roth, E. E. Scherer, C. Maden, K. Mezger and B. Bourdon, *Chemical Geology*, 2014, **386**, 238-248.

View Article Online
DOI: 10.1039/C9JA00308H

ARTICLE

Figures

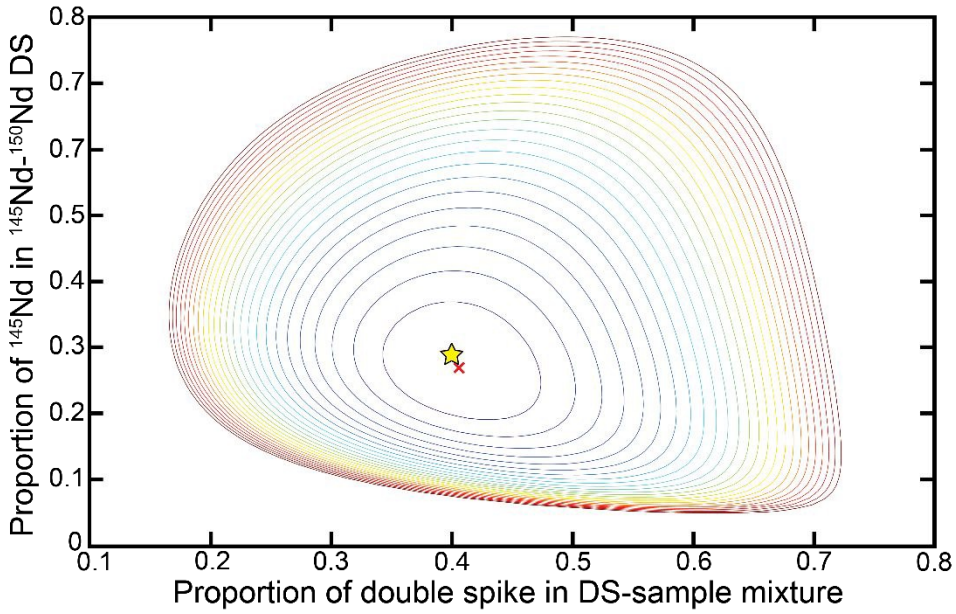

Figure 1: Contour plot showing the uncertainty (1 sd) in the natural fractionation factor (α) for a ^{145}Nd-^{150}Nd double spike (DS) when using ^{144}Nd, ^{145}Nd, ^{146}Nd and ^{150}Nd in the DS inversion. Uncertainty modelling is based on the calculations of Rudge et al. (2009) [36] using Oak Ridge National Laboratory spike compositions, with the optimum composition marked by a cross. The spike calibrated herein (star) consists of 28.5% ^{145}Nd and 65.7% ^{150}Nd and is plotted at the ideal spike to sample ratio (40:60) implemented in this study. The plot is thresholded so that only contours within 25 % of the optimal uncertainty are shown, and contours are evenly spaced with intervals of 1 % the optimal uncertainty on α.

Journal of Analytical Atomic Spectrometry ARTICLE

View Article Online
DOI: 10.1039/C9JA00308H

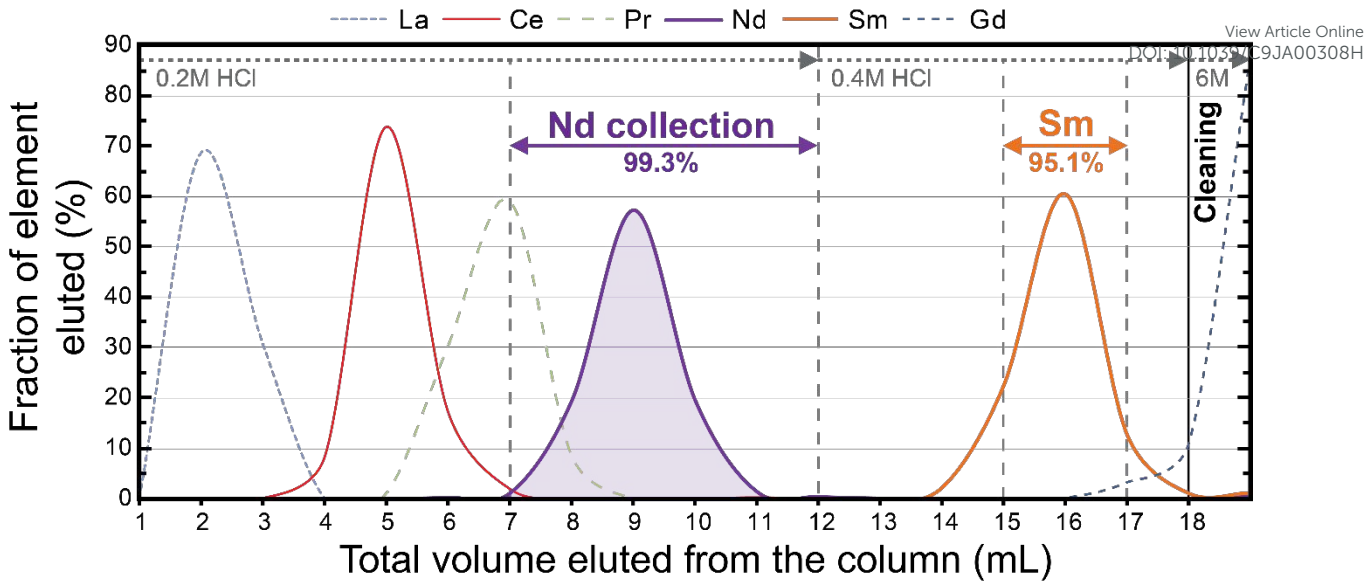

Figure 2: Representative elution curves showing the separation of the lanthanides using Ln-spec columns. Profile is generated from a 200 mg digestion of the USGS rock standard BCR-1. Sample was loaded in 0.5 mL of 0.2M HCl and then every millilitre subsequently eluted was collected and measured. After the 12th mL the acid molarity was increased to 0.4M HCl. Following the 18th mL cleaning the column commenced, this fraction represents the elution of 12 mL of 6M HCl.

View Article Online
DOI: 10.1039/C9JA00308H

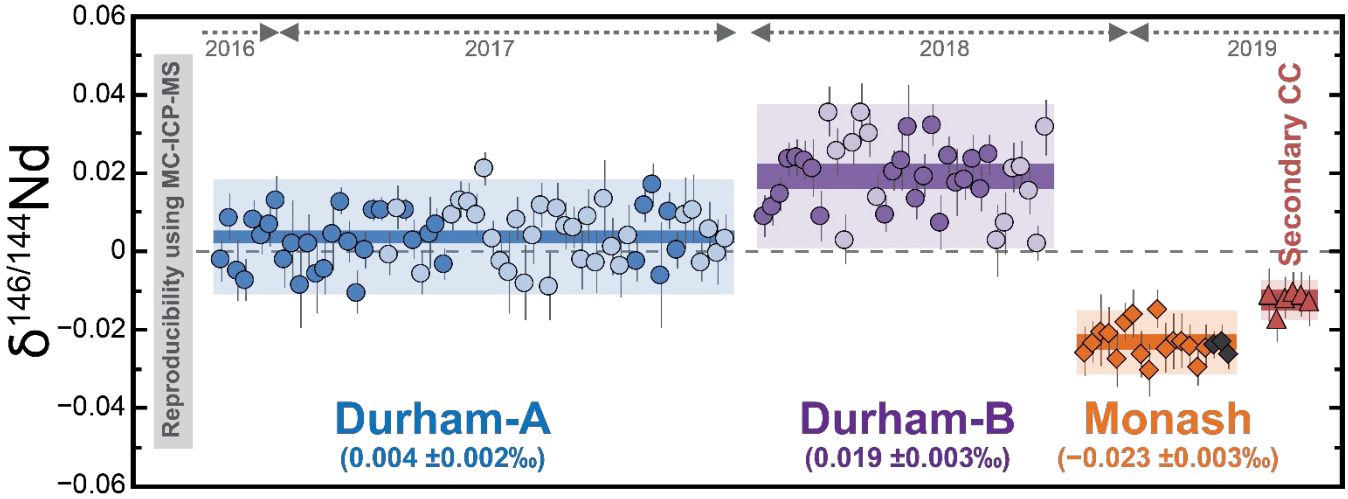

Figure 3: Long-term TIMS reproducibility of the JNdi-1 primary reference standard. At Durham University (circles: dark = 200 ng; light = 100 ng) from November 2016 to November 2017 (Durham-A) the δ^{146}Nd of JNdi-1 has an average composition of 0.004 ±0.002‰ (n = 64; ±0.014‰ 2sd). From January 2018 onwards (Durham-B), a new higher average value is then observed of δ^{146}Nd = 0.019 ±0.003‰ (n = 36; ±0.018‰ 2sd). At Monash University (diamonds) analyses of JNdi-1 from September 2018 to July 2019 (150 ng) show a resolvably lighter value with δ^{146}Nd = −0.023 ± 0.002‰ (n = 19; 0.008‰ 2sd). Black diamonds are analyses using amplifier rotation. Testing of a secondary collector configuration (^{145}Nd Axial; Table 3) at Monash (triangles) produced a resolvably different JNdi-1 value with δ^{146}Nd = −0.012 ± 0.003‰ (n = 6; ±0.005‰ 2sd). The complete dataset can be obtained from the electronic appendix. Darker shaded areas represent the 95% standard error of the mean (95% se), with the lighter shading showing the 2 standard deviations (2sd) of the population. Reproducibility of δ^{146}Nd using Neptune MC-ICP-MS is ±0.05‰ (2sd; BCR-2 n =5; [33]) is shown by the grey bar.

Journal of Analytical Atomic Spectrometry ARTICLE

View Article Online
DOI: 10.1039/C9JA00308H

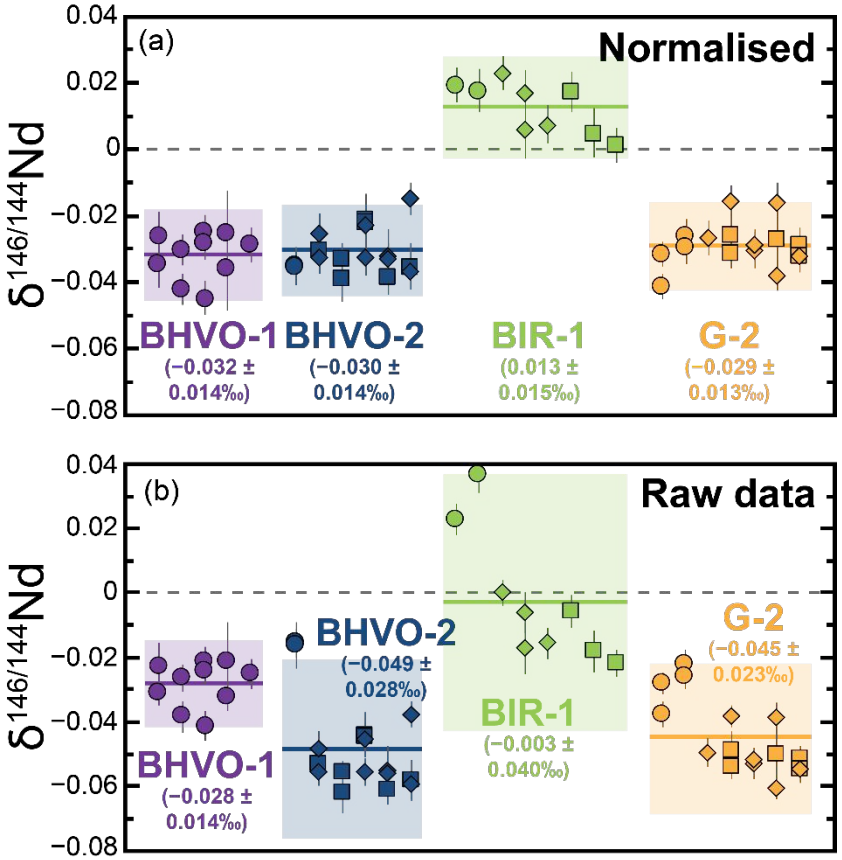

Figure 4: Long-term TIMS reproducibility (2 sd) of United States Geological Survey rock standards processed through the complete chemical separation protocol. Circles and diamonds represent samples processed with only the Nd DS at Durham University and Monash University, respectively. Squares represent samples processed at Monash University using both the NdDS and Sm tracer spike. (a) δ^{146}Nd values have been normalised for the long-term offset measured in JNdi-1 for a specific analytical period, so that JNd-1 = 0‰. Uncertainties were propagated in quadrature using the measured 2 se of the analysis and 95% se on the long-term average of the JNdi-1 from a specific period. (b) Raw measured δ^{146}Nd not corrected for offsets between analytical measurement sessions.

View Article Online
DOI: 10.1039/C9JA00308H

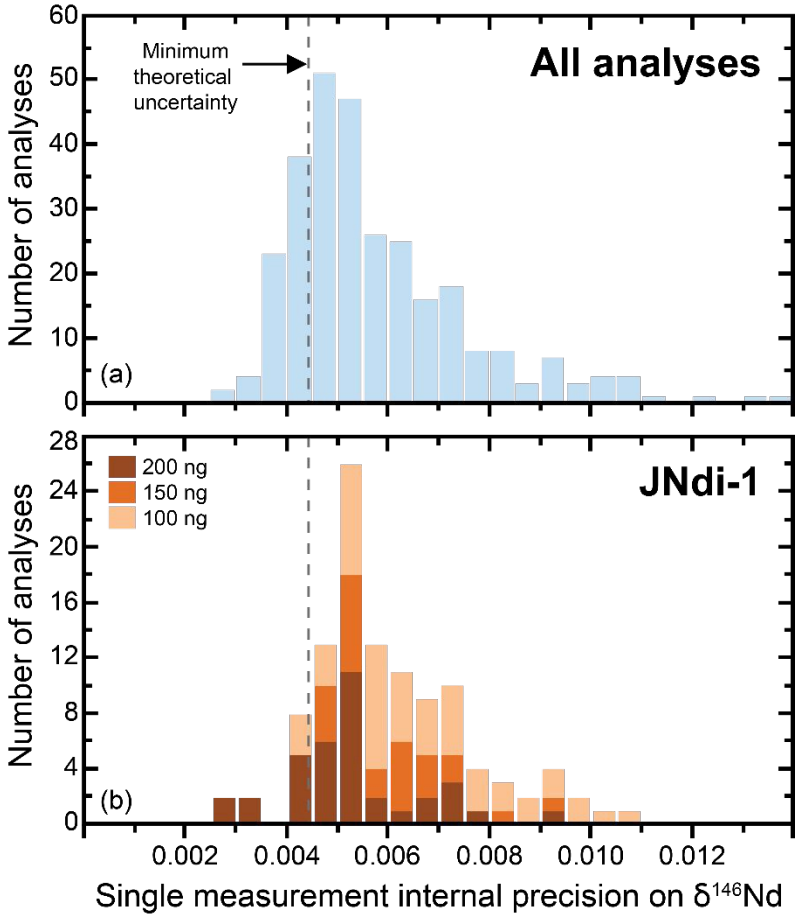

Figure 5: (a) Internal precision on δ^{146}Nd (‰) for all single measurements included in this study (n = 291; includes the data previously published in McCoy-West[30]). Minimum theoretical internal uncertainties are calculated using the uncertainty model of Rudge[36], based on a total Nd beam of 40 V (for the 4 isotopes involved in the DS deconvolution; ca. 6.5 V on ^{146}Nd) and 400 measurements of 8 second integrations. (b) Internal precision of δ^{146}Nd on the JNdi-1 standard for various quantities of loaded Nd. Filament loads of 100 ng (n = 50), 150 ng (n = 25) and 200 ng (n = 36) all consistently produce precisions of better than 0.008‰.

Journal of Analytical Atomic Spectrometry ARTICLE

View Article Online
DOI: 10.1039/C9JA00308H

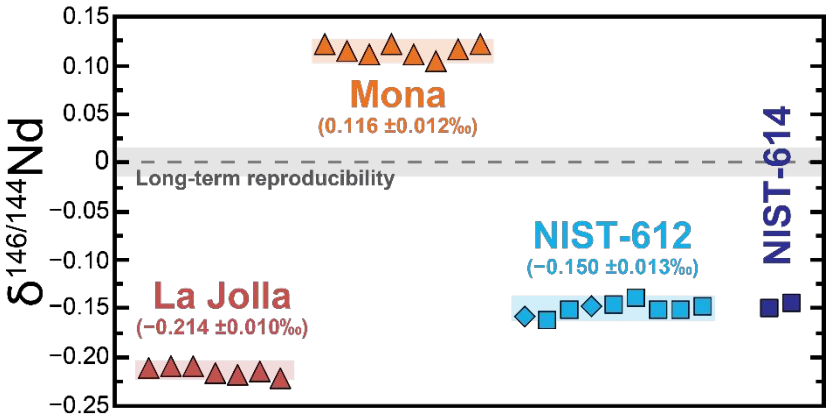

Figure 6: Reproducibility (2 sd) of synthetic reference materials. La Jolla and Mona are synthetic solutions (150 ng loaded per filament) that were not processed through chemistry. Synthetic glasses NISTSRM-612 (Nd = 34.87 ppm) and NISTSRM-614 (Nd = 0.743 ppm; δ^{146}Nd = −0.146 ± 0.007‰) were processed through the complete chemical separation protocol. Diamonds are aliquots with only Nd DS, whereas squares represent samples processed with both the NdDS and Sm tracer spike. For comparison the long-term reproducibility of δ^{146}Nd based on rock standards here (± 0.015‰) is also shown.

View Article Online
DOI: 10.1039/C9JA00308H

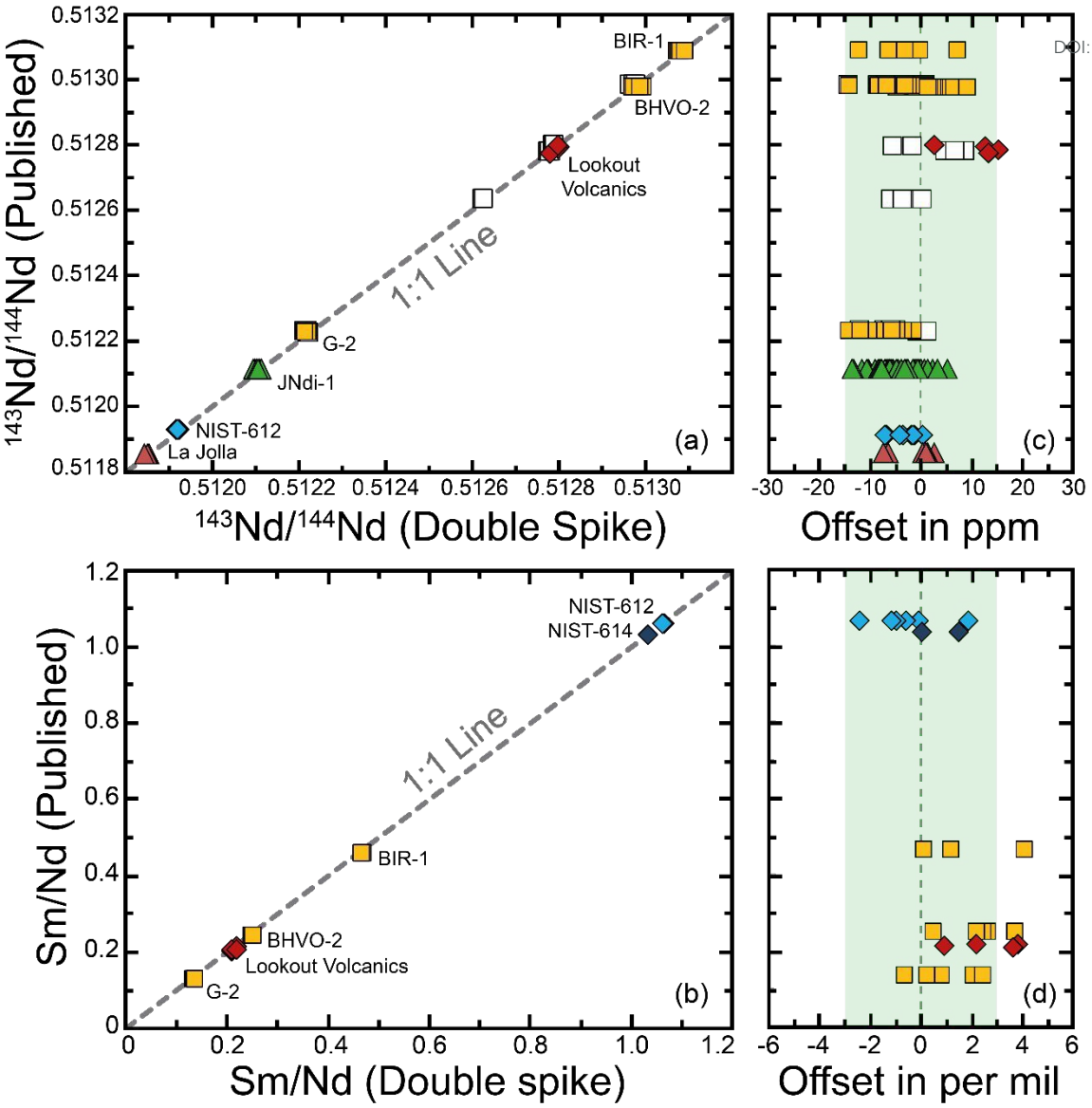

Figure 7: Comparison of ^{143}Nd/^{144}Nd isotope compositions (a) and Sm/Nd ratios (b) of previous published analyses and those obtained here following DS deconvolution. Published values come from [11, 55, 63, 64, 71]. Coloured symbols are analyses herein with rock standards analysed previously[30] shown as white squares. The offset in ^{143}Nd/^{144}Nd in parts per million (c) and Sm/Nd in per mil (d) from the published value is also shown. The shaded bar represents the long-term reproducibility of ±15 ppm on ^{143}Nd/^{144}Nd and ±0.3 % on Sm-Nd ratios.

Journal of Analytical Atomic Spectrometry ARTICLE

View Article Online
DOI: 10.1039/C9JA00308H

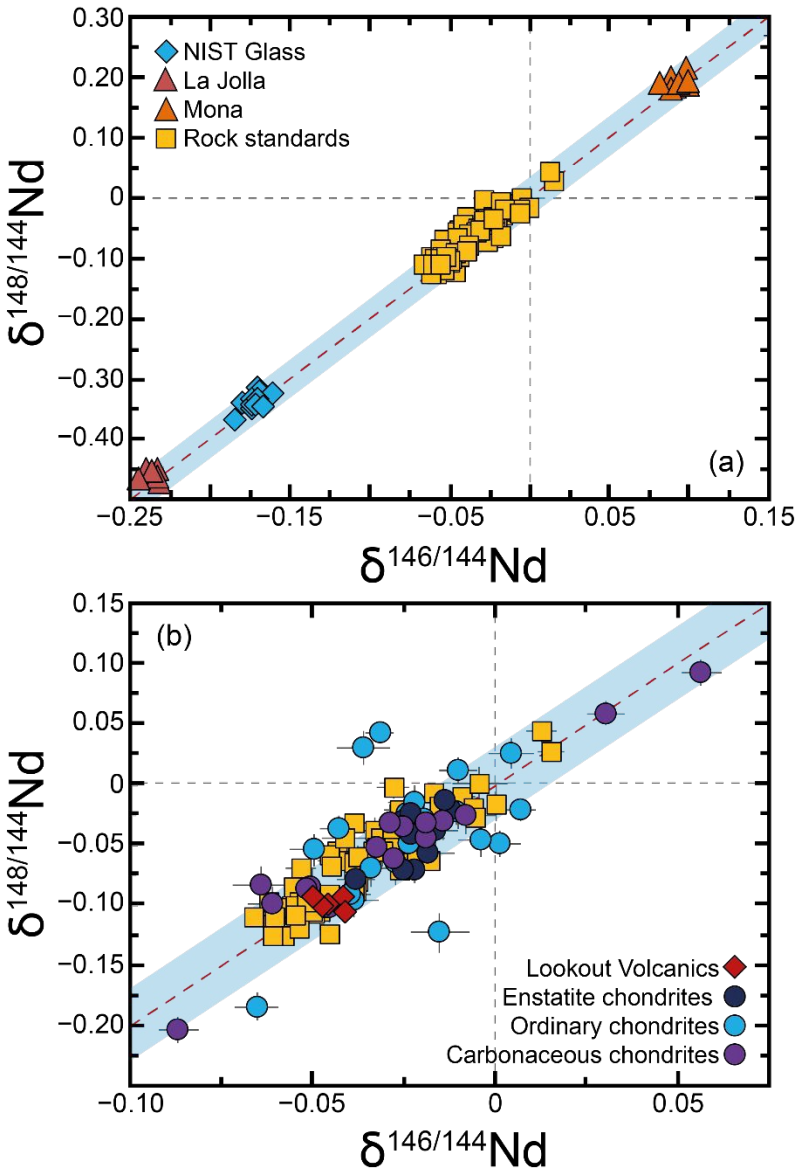

Figure 8: Plot showing the mass dependent covariation between δ^{146}Nd and δ^{148}Nd for reference standards (a) and rock matrices (b) measured in this study and McCoy-West et al. [30]. The red dashed line represents the theoretical mass dependent fractionation line with a slope of 2.00037, with the shaded field representing the long-term reproducibility on δ^{148}Nd of ±0.038‰, which is based on the long-term uncertainty on δ^{146}Nd (±0.015‰) but has been increased proportionally based on the relative mass difference between the isotopes and the less precise counting statistics due to the smaller ion beam on ^{148}Nd. All analyses exhibit mass dependence except a few chondritic meteorites.

View Article Online
DOI: 10.1039/C9JA00308H

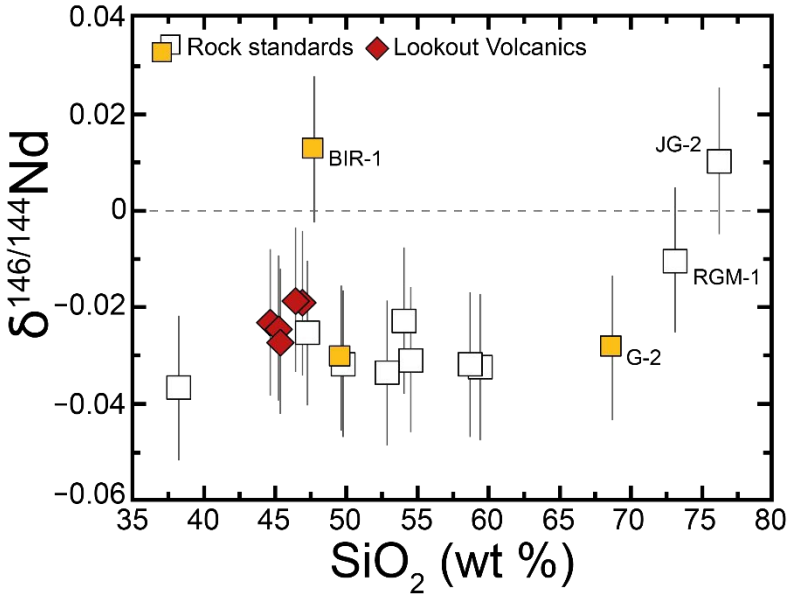

Figure 9: Graph showing the variability of δ^{146}Nd in terrestrial magmatic rocks versus SiO_2 content. Major element compositions come from [63] and [11]. Coloured symbols are analyses herein with rock standards analysed previously[30] shown as white squares.

Journal of Analytical Atomic Spectrometry ARTICLE

View Article Online
DOI: 10.1039/C9JA00308H

Table 1: Neodymium isotope ratios of reference standard JNdi-1 and the ^{145}Nd-^{150}Nd double spike used in this study.

	n	^{142}Nd/^{144}Nd	^{143}Nd/^{144}Nd	^{145}Nd/^{144}Nd	^{146}Nd/^{144}Nd	^{148}Nd/^{144}Nd	^{150}Nd/^{144}Nd
JNdi-1 Reference Standard							
Rizo et al. (2011)[64]	*21*	1.141837 ±5	0.512112 ±5	0.348416 ±4	0.7219	0.241591 ±4	0.236464 ±5
Roth et al. (2014)[86]	*7*	1.141836 ±5	0.512093 ± 6	0.348473 ±33	0.7219	0.241596 ± 15	0.236478 ± 34
Garcon et al. (2018)[56]	*61*	1.141832 ± 6	0.512099 ± 5	0.348403 ± 3	0.7219	0.241581 ± 3	0.236452 ± 6
^{145}Nd-^{150}Nd spike	*9*	0.336049 ± 9	0.225743 ± 5	19.4423 ± 1	2.21315 ± 2	0.158842 ± 5	44.7617 ± 8

The values of JNdi-1 are normalised to ^{146}Nd/^{144}Nd to correct for mass bias, with the quoted uncertainty representing the 2 sd. Here we use the values of Rizo et al. (2011)[64] to calibrate our double spike, which are within error of other recent estimates [56, 86].

The error on the DS is the relative 2 se on the analyses used to obtain the DS composition (based on 9 JNdi-DS mixtures).

Table 2: Samarium isotope ratios of reference standard Choice Sm and the ^{149}Sm tracer spike used in this study. External normalisation results of Sm spike

	^{144}Sm/^{152}Sm	^{147}Sm/^{152}Sm	^{148}Sm/^{152}Sm	^{149}Sm/^{152}Sm	^{150}Sm/^{152}Sm	^{154}Sm/^{152}Sm
Reference Std[A]	0.115217	0.561531	0.420867	0.517240	0.276132	0.850365
%SE	0.0127	0.0078	0.0063	0.0047	0.0031	0.0031
Recommended[B]	0.114927	0.560667	0.420333	0.516747	0.275954	0.850793
External f. f. [C]	0.99748	0.99846	0.99873	0.99905	0.99936	1.00050
% frac. Amu[D]	-0.031	-0.031	-0.032	-0.032	-0.032	-0.025
^{149}Sm spike[E]	0.024544	0.349798	1.759266	136.0183	3.429778	0.402880
%SE	0.0296	0.0148	0.0116	0.0087	0.0058	0.0059
^{149}Sm spike Norm[F]	0.024482	0.349039	1.755897	135.8009	0.342535	0.402467

A) Measured ratios of the normal Sm (High Purity Standards) without normalisation B) Recommended isotope ratios of normal Sm from [52] C) External fractionation factor D) Percentage fractionation per atomic mass unit E) Spike ratios measured with no normalisation F) Externally normalised ratios of the Sm spike.

View Article Online
DOI: 10.1039/C9JA00308H

Table 3: Faraday cup configurations used for Nd and Sm isotope measurements by static multi-collection using both TIMS and MC-ICP-MS. The secondary Nd cup configuration was employed at Monash University to test the effect of small offsets due to differences in faraday collector efficiency.

Cup	L4	L3	L2	L1	Ax	H1	H2	H3	H4
Neodymium									
Analyte Isotopes	^{142}Nd	^{143}Nd	^{144}Nd	^{145}Nd	^{146}Nd	^{147}Sm	^{148}Nd	^{150}Nd	
Isobars	^{142}Ce		^{144}Sm				^{148}Sm	^{150}Sm	
Secondary Configuration		*^{142}Nd*	*^{143}Nd*	*^{144}Nd*	*^{145}Nd*	*^{146}Nd*	*^{147}Sm*	*^{148}Nd*	*^{150}Nd*
Samarium									
Analyte Isotopes	^{144}Sm	^{146}Nd	^{147}Sm	^{148}Sm	^{149}Sm	^{150}Sm	^{152}Sm	^{154}Sm	^{155}Gd
Isobars	^{144}Nd			^{148}Nd		^{150}Nd	^{152}Gd	^{154}Gd	

Table 4: Reproducibility of Nd isotope measurements of pure reference solutions.

Sample	^{143}Nd/^{144}Nd	$\delta^{146/144}$Nd	$\delta^{148/144}$Nd	$\delta^{146}Nd_{COR}$	*n*
La Jolla-01	0.511859 ±3	−0.233 ±0.005	−0.448 ±0.009	−0.210 ±0.006	
La Jolla-02	0.511857 ±3	−0.232 ±0.005	−0.471 ±0.009	−0.209 ±0.006	
La Jolla-03	0.511856 ±3	−0.232 ±0.005	−0.462 ±0.010	−0.209 ±0.006	
La Jolla-04	0.511850 ±3	−0.239 ±0.005	−0.453 ±0.009	−0.216 ±0.006	
La Jolla-05	0.511857 ±3	−0.241 ±0.005	−0.448 ±0.011	−0.218 ±0.006	
La Jolla-06	0.511857 ±3	−0.237 ±0.005	−0.452 ±0.011	−0.214 ±0.006	
La Jolla-07	0.511849 ±3	−0.245 ±0.004	−0.465 ±0.008	−0.222 ±0.005	
Average	**0.511855 ±8**	**−0.237 ±0.010**	**−0.457 ±0.018**	**−0.214 ±0.010**	***7***
Published	*0.511856 ±7 (24)*			*−0.197 ±0.023 (2)*	
Mona-01	0.511551 ±3	0.099 ±0.006	0.217 ±0.012	0.122 ±0.007	
Mona-02	0.511559 ±3	0.092 ±0.005	0.185 ±0.010	0.115 ±0.006	
Mona-03	0.511550 ±3	0.089 ±0.005	0.200 ±0.010	0.112 ±0.006	
Mona-04	0.511554 ±3	0.099 ±0.006	0.188 ±0.011	0.122 ±0.006	
Mona-05	0.511554 ±3	0.089 ±0.005	0.182 ±0.011	0.112 ±0.006	
Mona-06	0.511554 ±3	0.082 ±0.010	0.192 ±0.021	0.105 ±0.011	
Mona-07	0.511555 ±3	0.093 ±0.005	0.190 ±0.010	0.116 ±0.006	
Mona-08	0.511559 ±3	0.099 ±0.006	0.195 ±0.011	0.122 ±0.006	
Average	**0.511559 ±11**	**0.093 ±0.012**	**0.194 ±0.022**	**0.116 ±0.012**	***8***

Each analysis represents a separate filament load. Uncertainties on averages are 2 standard deviations. Comparative data for La Jolla from [31, 55]. $\delta^{146}Nd_{COR}$ values have been corrected to JNdi-1 = 0‰ and uncertainties have been propagated. All ^{143}Nd/^{144}Nd have been corrected to ^{143}Nd/^{144}Nd in JNdi-1 = 0.512112[64]. All these analyses were undertaken at Monash University.

Journal of Analytical Atomic Spectrometry ARTICLE

Table 5: Neodymium isotope compositions and Sm-Nd ratios of rock standards, synthetic glass and a suite of intraplate basalts.

View Article Online
DOI: 10.1039/C9JA00308H

Sample		Nd (ppm)	Sm (ppm)	Sm/Nd	$^{143}Nd/^{144}Nd$	$\delta^{146}Nd$	$\delta^{148}Nd$	$\delta^{146}Nd_{COR}$
USGS Rock Standards								
BHVO-2 (1)	D2	24.17			0.512988 ±3	-0.016 ±0.004	-0.067 ±0.009	-0.035 ±0.005
BHVO-2 (1)*	D2	24.17			0.512994 ±4	-0.016 ±0.007	-0.073 ±0.015	-0.035 ±0.008
BHVO-2 (2)	M	24.82			0.512978 ±3	-0.048 ±0.005	-0.105 ±0.010	-0.025 ±0.006
BHVO-2 (2)#	M	24.76			0.512981 ±2	-0.056 ±0.004	-0.106 ±0.008	-0.033 ±0.005
BHVO-2 (2)$	M	24.22	6.022	0.2486	0.512979 ±3	-0.053 ±0.006	-0.069 ±0.012	-0.030 ±0.007
BHVO-2 (3)$	M	23.93	6.029	0.2519	0.512979 ±4	-0.062 ±0.006	-0.097 ±0.013	-0.039 ±0.007
BHVO-2 (3)$	M	24.13	6.052	0.2508	0.512976 ±2	-0.056 ±0.004	-0.107 ±0.008	-0.033 ±0.005
BHVO-2 (4)	M	24.75			0.512984 ±4	-0.045 ±0.005	-0.124 ±0.010	-0.022 ±0.006
BHVO-2 (4)#	M	24.64			0.512981 ±2	-0.056 ±0.004	-0.106 ±0.008	-0.033 ±0.005
BHVO-2 (4)$	M	24.04	6.021	0.2504	0.512985 ±4	-0.044 ±0.007	-0.097 ±0.014	-0.021 ±0.008
BHVO-2 (4)$	M	24.06	6.030	0.2506	0.512986 ±3	-0.045 ±0.006	-0.068 ±0.012	-0.022 ±0.007
BHVO-2 (5)	M	25.08			0.512981 ±3	-0.055 ±0.008	-0.085 ±0.015	-0.032 ±0.008
BHVO-2 (5)#	M	25.11			0.512974 ±2	-0.056 ±0.004	-0.101 ±0.008	-0.033 ±0.005
BHVO-2 (5)$	M	24.12	6.039	0.2504	0.512978 ±3	-0.061 ±0.005	-0.116 ±0.010	-0.038 ±0.006
BHVO-2 (6)	M	24.82			0.512979 ±2	-0.060 ±0.004	-0.101 ±0.009	-0.037 ±0.005
BHVO-2 (6)#	M	24.78			0.512988 ±2	-0.038 ±0.004	-0.080 ±0.008	-0.015 ±0.005
BHVO-2 (6)$	M	24.02	5.999	0.2498	0.512978 ±4	-0.058 ±0.006	-0.125 ±0.013	-0.035 ±0.007
Average		**24.44 ±0.81**	**6.027 ±0.033**	**0.250 ±0.002**	**0.512982 ±10**	**-0.048 ±0.027**		**-0.030 ±0.014**
Published Av.		*24.27 ±0.25*	*6.023 ±0.009*	*0.248 ±0.004*	*0.512983 ±5*			
BIR-1 (1)	D1	2.269	-	-	0.513088 ±3	0.023 ±0.005	0.026 ±0.010	0.019 ±0.005
BIR-1 (2)	D2	2.367	-	-	0.513098 ±3	0.037 ±0.006	0.055 ±0.011	0.018 ±0.007
BIR-1 (3)	M	2.342	-	-	0.513090 ±2	0.000 ±0.004	-0.017 ±0.008	0.023 ±0.005
BIR-1 (4)	M	2.342	-	-	0.513079 ±5	-0.017 ±0.008	-0.008 ±0.016	0.006 ±0.009
BIR-1 (4)*	M	2.342	-	-	0.513088 ±4	-0.006 ±0.006	-0.019 ±0.012	0.017 ±0.007
BIR-1 (5)	M	2.338	-	-	0.513085 ±3	-0.016 ±0.005	-0.018 ±0.010	0.007 ±0.006
BIR-1 (6)$	M	2.336	1.085	0.4645	0.513088 ±3	-0.006 ±0.005	-0.027 ±0.010	0.017 ±0.006
BIR-1 (7)$	M	2.329	1.091	0.4684	0.513091 ±4	-0.018 ±0.007	-0.063 ±0.013	0.005 ±0.007
BIR-1 (8)$	M	2.325	1.082	0.4655	0.513085 ±2	-0.022 ±0.004	-0.034 ±0.009	0.001 ±0.005
Average		**2.332 ±0.053**	**1.086 ±0.009**	**0.466 ±0.004**	**0.513088 ±11**	**-0.003 ±0.040**		**0.013 ±0.015**
Published Av.		*2.397± 0.043*	*1.113 ±0.016*	*0.464 ±0.011*	*0.513096 ±18*			
G-2 (1)	D1	53.53			0.512221 ±2	-0.028 ±0.003	-0.003 ±0.007	-0.032 ±0.004
G-2 (1)*	D1	53.54			0.512228 ±2	-0.038 ±0.004	-0.059 ±0.008	-0.041 ±0.004
G-2 (2)	D1	53.89			0.512226 ±3	-0.022 ±0.005	-0.031 ±0.009	-0.026 ±0.005
G-2 (2)*	D1	53.89			0.512227 ±2	-0.026 ±0.004	-0.036 ±0.008	-0.029 ±0.005
G-2 (3)	M	54.22			0.512226 ±3	-0.050 ±0.004	-0.108 ±0.009	-0.027 ±0.005
G-2 (4)	M	53.62			0.512232 ±2	-0.038 ±0.003	-0.088 ±0.007	-0.015 ±0.005
G-2 (4)$	M	52.95	7.184	0.1357	0.512228 ±2	-0.049 ±0.006	-0.102 ±0.012	-0.026 ±0.007
G-2 (4)$	M	52.73	7.176	0.1361	0.512225 ±2	-0.054 ±0.004	-0.097 ±0.007	-0.031 ±0.005
G-2 (5)	M	54.09			0.512224 ±2	-0.053 ±0.004	-0.105 ±0.009	-0.030 ±0.005
G-2 (5)#	M	54.10			0.512226 ±2	-0.052 ±0.004	-0.097 ±0.008	-0.029 ±0.005
G-2 (6)	M	53.64			0.512222 ±2	-0.061 ±0.004	-0.110 ±0.007	-0.038 ±0.005
G-2 (6)#	M	53.73			0.512230 ±3	-0.039 ±0.005	-0.088 ±0.010	-0.016 ±0.006
G-2 (6)$	M	54.05	7.186	0.1330	0.512225 ±3	-0.050 ±0.008	-0.105 ±0.016	-0.027 ±0.008
G-2 (7)	M	53.86			0.512223 ±2	-0.055 ±0.004	-0.101 ±0.008	-0.032 ±0.005
G-2 (7)#	M	53.61	7.209	0.1345	0.512227 ±2	-0.052 ±0.004	-0.098 ±0.008	-0.029 ±0.005
G-2 (7)$	M	53.91	7.216	0.1339	0.512219 ±2	-0.055 ±0.004	-0.109 ±0.008	-0.032 ±0.005
Average		**53.71 ±0.80**	**7.194 ±0.035**	**0.135 ±0.003**	**0.512226 ±7**	**-0.045 ±0.023**		**-0.029 ±0.013**
Published Av.		*53.81 ±0.67*	*7.19 ±0.10*	*0.133 ±0.003*	*0.512225 ±16*			
NISTSRM Glass								
NIST-612 (1)	M	34.69			0.511904 ±3	-0.180 ±0.005	-0.338 ±0.009	-0.157 ±0.005
NIST-612 (1)$	M	34.65	36.80	1.0621	0.511909 ±5	-0.184 ±0.007	-0.366 ±0.013	-0.161 ±0.007
NIST-612 (1)$	M	34.76	36.86	1.0602	0.511907 ±3	-0.174 ±0.005	-0.348 ±0.009	-0.151 ±0.005
NIST-612 (2)	M	34.97			0.511904 ±2	-0.170 ±0.004	-0.314 ±0.008	-0.147 ±0.005
NIST-612 (2)$	M	35.09	37.28	1.0625	0.511910 ±2	-0.169 ±0.004	-0.321 ±0.007	-0.146 ±0.005
NIST-612 (3)$	M	34.94	37.19	1.0646	0.511911 ±3	-0.161 ±0.005	-0.324 ±0.010	-0.138 ±0.006

View Article Online
DOI: 10.1039/C9JA00308H

NIST-612 (3)$	M	35.00	37.17	1.0621	0.511908 ±3	-0.173 ±0.005	-0.334 ±0.010	-0.150 ±0.006
NIST-612 (4)$	M	34.89	37.04	1.0617	0.511909 ±2	-0.173 ±0.004	-0.343 ±0.009	-0.150 ±0.005
NIST-612 (4)$	M	34.88	37.03	1.0615	0.511907 ±2	-0.170 ±0.004	-0.333 ±0.007	-0.147 ±0.005
Average		**34.87± 0.29**	**37.05 ±0.35**	**1.062 ±0.003**	**0.511908 ±5**			**-0.150 ±0.013**
Published		*34.96 ±0.63*	*37.15 ±0.56*	*1.062 ±0.003*	*0.511911 ±13*			
NIST-614 (1)$	M	0.735	0.760	1.0341	0.511908 ±3	-0.171 ±0.006	-0.343 ±0.012	-0.148 ±0.007
NIST-614 (2)$	M	0.752	0.776	1.0326	0.511910 ±3	-0.166 ±0.006	-0.345 ±0.011	-0.143 ±0.006
Average		**0.743 ±0.024**	**0.768 ±0.023**	**1.033 ±0.002**	**0.511909 ±4**			**-0.146 ±0.007**
Published		*0.740*	*0.761*	*1.033*				
Lookout Volcanics								
AMB-10	M	20.22	4.414	0.2183	0.512811 ±3	-0.046 ±0.004	-0.100 ±0.009	-0.023 ±0.005
AMB-22	M	21.27	4.680	0.2200	0.512804 ±2	-0.047 ±0.004	-0.100 ±0.008	-0.024 ±0.005
AMB-41	M	34.05	7.090	0.2082	0.512788 ±3	-0.042 ±0.004	-0.092 ±0.009	-0.019 ±0.005
AMC-9	M	29.99	6.303	0.2102	0.512788 ±2	-0.042 ±0.004	-0.105 ±0.007	-0.019 ±0.005
AMG-8	M	29.72	6.454	0.2172	0.512804 ±2	-0.050 ±0.004	-0.093 ±0.007	-0.027 ±0.005

Uncertainties on measured $^{143}Nd/^{144}Nd$ and $\delta^{146}Nd$ and $\delta^{148}Nd$ are 2 standard errors. () Numbers in parentheses represent a separate digestion. * represents a duplicate analysis on a different filament. # represents an independent processing of a spiked aliquot through the chemical separation protocol. $ denotes samples that also have the Sm tracer spike added. Column 2 refers to the analysis period (see Fig. 3): M = Monash; D1 = Durham-A; D2 = Durham-B. Uncertainties on averages are 2 standard deviations. Comparative data is taken from for the rock standards and [69-71] for NIST glasses. See electronic supplementary material values used in calculation of averages. $\delta^{146}Nd_{COR}$ values are were measured $\delta^{146}Nd$ has been corrected to JNdi-1 = 0‰ and uncertainties have been propagated. All $^{143}Nd/^{144}Nd$ have been corrected to $^{143}Nd/^{144}Nd$ in JNdi-1 = 0.512112[64].

View Article Online
DOI: 10.1039/C9JA00308H

We present a method for the determination of $\delta^{146}Nd$, $^{143}Nd/^{144}Nd$ and Sm-Nd ratios from a single measurement.

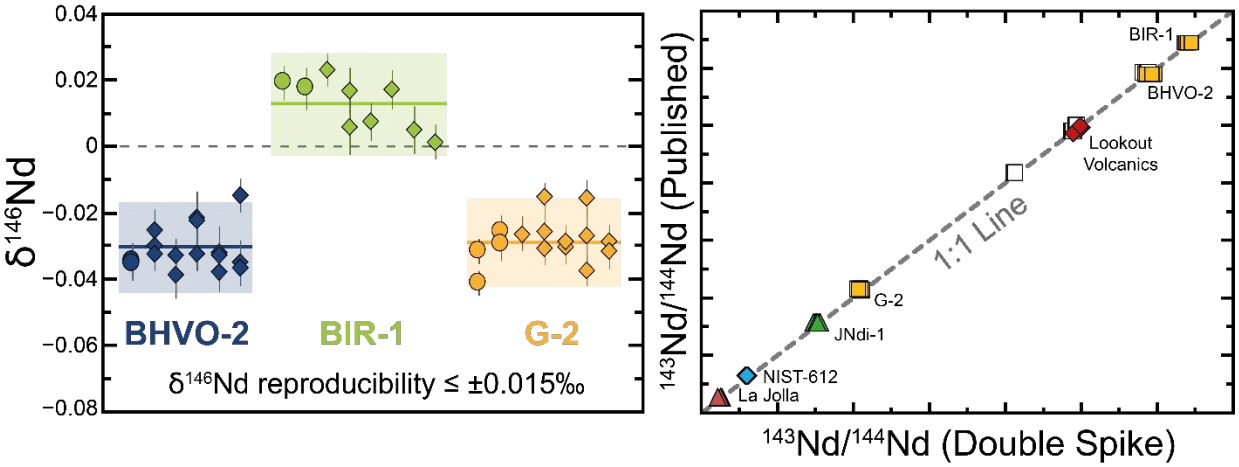

View Article Online
DOI: 10.1039/C9JA00308H

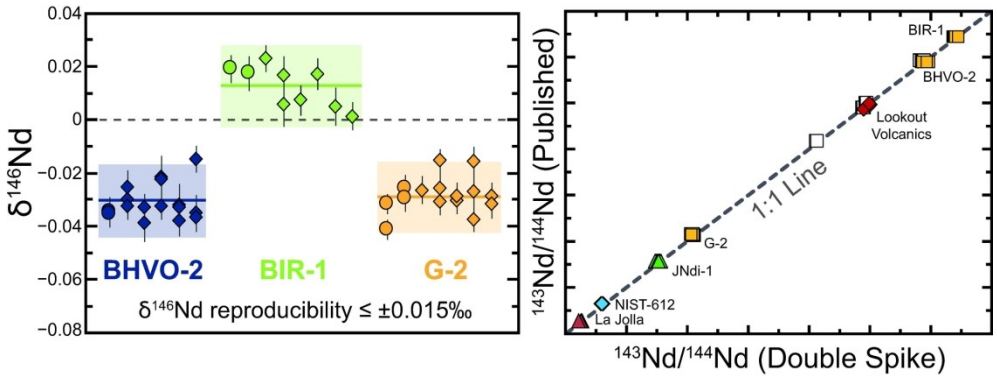

Graphical Abstract

198x73mm (300 x 300 DPI)